Available online at www.sciencedirect.com
SCIENCE DIRECT®
Journal of Sound and Vibration 286 (2005) 265–312
JOURNAL OF SOUND AND VIBRATION
www.elsevier.com/locate/jsvi

New insight into and simplified approach to seismic analysis of torsionally coupled one-story, elastic systems

T.L. Trombetti[a], J.P. Conte[b,*]

[a]*Dipartimento D.I.S.T.A.R.T., Facolta' di Ingegneria, Universita' degli Studi di Bologna, Viale Risorgimento 2, 40136 Bologna, Italy*
[b]*Department of Structural Engineering, University of California at San Diego, 9500 Gilman Drive, La Jolla, CA 92093-0085, USA*

Received 14 August 2001; received in revised form 24 September 2004; accepted 5 October 2004
Available online 13 January 2005

Abstract

Structures characterized by non-coincident center of mass and center of stiffness, referred to herein as eccentric structures, develop a coupled lateral–torsional response when subjected to dynamic excitation. This phenomenon is particularly important for seismic isolated structures due to the potentially large deformations imposed on the seismic isolators by the earthquake ground motion.

A careful examination of the governing equations of motion of linear elastic, one-story eccentric systems sheds new light and new insight into the coupled lateral–torsional dynamic behavior of such systems and leads to the identification of a basic system parameter, the "alpha" parameter, which controls the maximum rotational response of such systems under free and forced vibrations. The "alpha" parameter is defined as the mass radius of gyration of the structure multiplied by the ratio of the maximum rotational to the maximum longitudinal displacement response developed by a one-story eccentric system under free vibration from a given initial deformation. Closed-form exact and approximate solutions for the "alpha" parameter are provided for undamped and damped eccentric systems, respectively, for a wide range of system parameters. A new basic result is that the "alpha" parameter has an upper bound of unity, thus physically limiting the maximum rotational response of an eccentric system in free vibration from an initial imposed deformation. A new physically based, simplified analysis procedure is developed, based on the "alpha" parameter to effectively estimate the maximum rotational response of a given eccentric system under seismic excitation. The extensive numerical and experimental verification of the simplified "alpha"

*Corresponding author.
E-mail addresses: tomaso.trombetti@mail.ing.unibo.it (T.L. Trombetti), jpconte@ucsd.edu (J.P. Conte).

0022-460X/$ - see front matter
doi:10.1016/j.jsv.2004.10.021

method performed demonstrate that the proposed "alpha" method is accurate enough for design purposes, is robust and is significantly more accurate than the current International Building Code (IBC) design provisions.

The experimental verification was performed through a suite of 88 shaking table tests performed on a versatile, carefully designed, one-story small-scale building model able to represent the dynamic characteristics of a wide range of eccentric systems.

The dimensionless "alpha" parameter, bounded between zero and unity, can also be used as a formal index for the inherent property of a given structure to develop a rotational response under dynamic excitation. Sensitivities of the "alpha" parameter to various physical system characteristics are investigated and provide valuable guidance for eccentric system design.

1. Introduction

The dynamic behavior of eccentric structures has been the object of extensive research since the late 1970s both in the linear and nonlinear domains. In spite of these research efforts, a number of issues remain unresolved in the areas of (1) inelastic response [1], and (2) development of simplified, yet accurate and physically based simplified design procedures.

The research in lateral–torsional coupling performed to date can be subdivided into three categories:

(1) Investigation of the linear elastic response of full 3D laterally–torsionally coupled structural systems [2–7]. These studies focus on the fundamentals of the dynamic behavior of linear elastic eccentric systems and on the identification of their controlling parameters.
(2) Investigation of the nonlinear inelastic dynamic response of 3D single and multi-story eccentric structural systems [1,8–14]. This body of research focuses mainly on the fundamental issue of evaluating the influence of the plan-wise distributions of stiffness and strength on the inelastic response of asymmetric building structures.
(3) Analysis and evaluation of design code provisions for torsional effects in building structures [1,7,15–22]. These studies include comparative analyses of different design code provisions [21,22] and development of improved rational design code provisions [7,22].

The analysis of the coupled lateral–torsional dynamic response of base-isolated building structures can be fairly simplified for the following reasons:

- Most common seismic isolators are cylindrical in shape with a well-defined lateral stiffness that is generally independent of the direction of deformation [6].
- It has been shown [6] that the dynamic behavior of seismic isolated structures can be fairly well captured through a simplified equivalent linear analysis in spite of the inherent nonlinear force–deformation relationship of most common seismic isolators.
- Under strong motion excitation, the deformations of a seismic isolated structure are localized mainly in the seismic isolators and are only marginally influenced by the dynamic interaction

with the superstructure [6,23,24]. This is especially true under design earthquake conditions with fully softened isolator stiffness. However, caution must be exercised in the case of small-to-moderate earthquakes for which a higher effective stiffness of the isolators leads to dynamic excitation of the superstructure [25].

For conceptual design purposes, the dynamic analysis of seismic isolated structures can be effectively reduced to that of a one story 3D linear structural system with a roof diaphragm/slab assumed infinitely stiff in its own plane (i.e., rigid diaphragm assumption). Since the maximum isolator deformation is the basic design parameter considered in design codes, it is essential to develop a simple, rational and reliable method to determine the local increase (as compared to the non-eccentric case) in the maximum isolator deformation due to eccentricity-induced rotational response.

Nagarajaiah et al. [24] confirmed that the superstructure has a small influence on the maximum deformation of base isolators and investigated the effects of selected parameters of eccentric structures on the dynamic coupled lateral–torsional response of base isolated systems. These results, however, are presented for a specific structural system and are not extended into a general purpose simplified theory. The new insight presented in this paper and the resulting simplified dynamic analysis procedure apply to a wide range of linear elastic base isolated systems and provide both a qualitative understanding and an effective quantitative estimate (for practical design purposes) of the effect of torsional coupling on their seismic response. The proposed approach provides a new simple, physically based formula to estimate the maximum rotational response of a given eccentric linear elastic one-story system in terms of few identified dimensionless controlling parameters of the system. The paper also provides extensive numerical and experimental (through shaking table tests) verifications of the proposed simplified approach referred to as the ''alpha'' method over a wide range of controlling system parameters.

The experimental verification is based on a large set of shaking table tests performed on a small-scale one-story building model carefully designed to accommodate a wide range of eccentricity of the center of stiffness relative to the center of mass of the system.

2. The eccentric dynamic system and its modes of vibration

Consider the 3D one-story system idealization with rigid in-plane diaphragm of a general base isolated structure with non-coincident center of mass and center of stiffness as shown in Fig. 1. In this idealization, the effects of rocking are neglected and the seismic isolators are considered axially inextensible. Also shown in this figure are the 3 dofs used in formulating the equations of motion. Note that these dofs are attached to the center of mass of the system.

Under the following two assumptions:

- the lateral stiffness ($k_i, i = 1, \ldots, N$) of each of the N base isolators does not depend on the direction of deformation; and
- the rotational response u_θ developed under dynamic (e.g., seismic) excitation is small enough so that $u_\theta \cong \sin(u_\theta) \cong \tan(u_\theta)$;

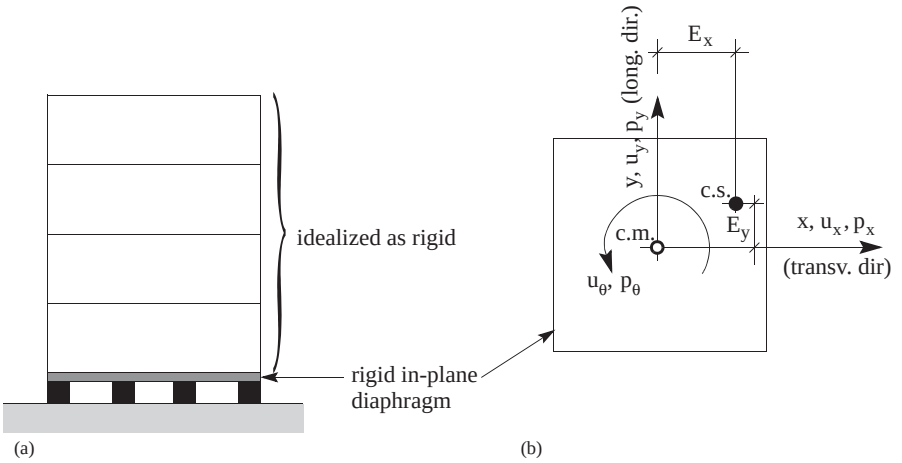

Fig. 1. One-story system idealization of an eccentric base isolated structure: (a) elevation; (b) plan view: ● = center of stiffness, ◯ = center of mass.

the dynamic coupled lateral–torsional response of the system considered is governed by the following set of coupled differential equations of motion [26,27]:

$$m\begin{bmatrix}\ddot{u}_x(t)\\ \ddot{u}_y(t)\\ \rho\ddot{u}_\theta(t)\end{bmatrix}+[C]\begin{bmatrix}\dot{u}_x(t)\\ \dot{u}_y(t)\\ \rho\dot{u}_\theta(t)\end{bmatrix}+m\omega_L^2\begin{bmatrix}1 & 0 & (-e_y\sqrt{12})\\ 0 & 1 & (e_x\sqrt{12})\\ (-e_y\sqrt{12}) & (e_x\sqrt{12}) & \gamma^2\end{bmatrix}\begin{bmatrix}u_x(t)\\ u_y(t)\\ \rho u_\theta(t)\end{bmatrix}$$
$$=\begin{bmatrix}1 & 0 & 0\\ 0 & 1 & 0\\ 0 & 0 & \frac{1}{\rho}\end{bmatrix}\begin{bmatrix}p_x(t)\\ p_y(t)\\ p_\theta(t)\end{bmatrix}, \tag{1}$$

where $u_x(t), u_y(t), u_\theta(t)$ are the translations along the x- and y- directions and rotation along the z-axis, respectively, of the base isolated system, m the total mass of the superstructure, i.e., total mass resting over the base isolators, I_p the polar mass moment of inertia of the superstructure with respect to the z-axis which passes through the center of mass, $\rho=\sqrt{I_p/m}$ the mass radius of gyration (or radius of inertia) of the superstructure with respect to the z-axis, x_i, y_i the x- and y-coordinates of the ith base isolator, k_i the lateral stiffness (in any direction) of the ith base isolator, $k=\sum_{i=1}^{N}k_i$ the lateral stiffness (in any direction) of the total base isolation system, $E_x=\left[\sum_{i=1}^{N}k_ix_i\right]/k, E_y=\left[\sum_{i=1}^{N}k_iy_i\right]/k$ the eccentricity in the x- and y-direction, respectively, of the center of stiffness of the total base isolation system with respect to the center of mass, $k_{\theta\theta}=\sum_{i=1}^{N}k_i(x_i^2+y_i^2)$ the rotational stiffness (about the z-axis) of the total base isolation system, $p_x(t), p_y(t), p_\theta(t)$ are the external dynamic forces/moment applied along the x-, y- and z-directions, respectively, $[C]$ the damping matrix, $\omega_L=\sqrt{k/m}$ the uncoupled lateral (longitudinal or

transversal) natural circular frequency of vibration, ω_L the lateral natural circular frequency of vibration of a structure similar to the one considered, but with coincident center of mass and center of stiffness, $\omega_\theta = \sqrt{k_{\theta\theta}/I_P}$ the natural circular frequency of rotational vibration of a fictitious non-eccentric structure having the same rotational stiffness and mass moment of inertia (with respect to the z-axis) as the eccentric system considered here, $\gamma = \omega_\theta/\omega_L = \sqrt{k_{\theta\theta}/\rho^2 k}$ the ratio of ω_θ defined above to the lateral uncoupled natural circular frequency, $D_e = \rho\sqrt{12}$ the "equivalent diagonal" of the system,[1] $e_x = E_x/D_e, e_y = E_y/D_e$ the relative eccentricity in the x- and y-direction, respectively.

In the case of a rectangular base isolated structure of size $L_m \times L_n$ with identical isolators located at the nodes of a regular rectangular $m \times n$ grid, the parameter γ can be shown to be [28].

$$\gamma = \frac{\omega_\theta}{\omega_L} = \sqrt{\frac{k_{\theta\theta}}{\rho^2 k}} = \sqrt{\frac{1}{L_m^2 + L_n^2}\left[L_m^2 \frac{m+2}{m} + L_n^2 \frac{n+2}{n}\right] + 12e^2}. \tag{2}$$

For base-isolated structures characterized by a 5 m × 5 m grid of regularly spaced isolators, γ can be fairly well estimated as $\gamma = \sqrt{1 + 13/D_e}$ with D_e expressed in meters [27]. Parameter γ, generally larger than one, tends to one as the number of base isolators increases within the given planar dimensions of the base isolation system (and assuming a fairly uniform distribution of the mass of the structure over its base).

Given the linear nature of the problem, it is possible, for undamped or classically damped systems, to uncouple the equations of motion in Eq. (1) through (second-order) modal analysis [29]. Considering that both the stiffness and damping of the system are derived from the isolators and that the stiffness and damping of an isolator, for a given height, are proportional to its size, it follows that, assuming viscous material damping, the damping matrix derived is proportional to the stiffness matrix. Therefore, classical damping is a reasonable assumption. Furthermore, it was shown that for nonclassically damped asymmetric-plan structures, the classical damping assumption can be used without introducing significant errors in the simulated response [30]. The solution of the eigenvalue problem governing the undamped free vibrations of the system gives the following natural circular frequencies ω_1, ω_2, and ω_3, normalized with respect to ω_L and squared:[2]

$$\Omega_1 = \left(\frac{\omega_1}{\omega_L}\right)^2 = \frac{1}{2}\left\{1 + \gamma^2 - \sqrt{(\gamma^2 - 1)^2 + 48e^2}\right\} = 1 + \frac{e}{2}\Theta_1, \tag{3a}$$

$$\Omega_2 = \left(\frac{\omega_2}{\omega_L}\right)^2 = 1, \tag{3b}$$

[1] The "equivalent diagonal" is a useful standard measure used herein to characterize the planar dimensions of the system. It is equal to $\sqrt{12}$ times the radius of inertia of the system. This length, for systems of rectangular shape and uniform mass distribution, coincides with the actual length of the diagonal of the system.

[2] In this paper, we considered and used for all plots the following ranges for the "e" and "γ" parameter values: $0 \leqslant e \leqslant 0.22$ and $1.0 \leqslant \gamma \leqslant 1.8$. However, most structures have a relative eccentricity "e" in the range between 0.03 (accidental eccentricity) and 0.07, and a "γ" parameter in the range between 1.1 and 1.3, leading to a parameter "F" ranging between 0.1 and 0.3.

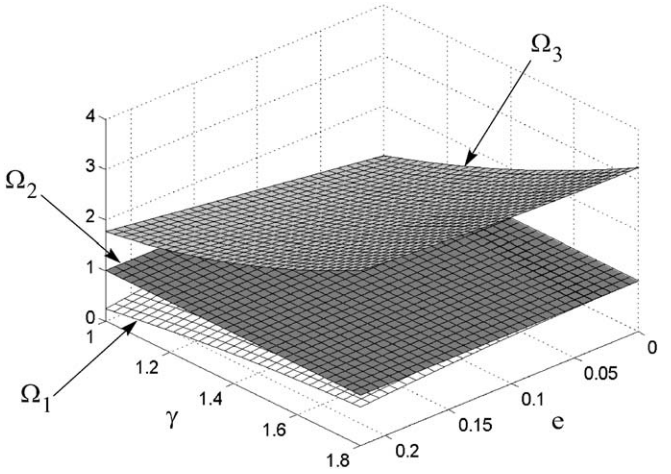

Fig. 2. Normalized undamped natural frequencies Ω_1, Ω_2, and Ω_3 versus structural parameters "e" and "γ".

$$\Omega_3 = \left(\frac{\omega_3}{\omega_L}\right)^2 = \frac{1}{2}\left\{1 + \gamma^2 + \sqrt{(\gamma^2 - 1)^2 + 48e^2}\right\} = 1 + \frac{e}{2}\Theta_3, \tag{3c}$$

where

$$e^2 = e_x^2 + e_y^2 \quad \text{and} \quad F = \frac{e}{\gamma^2 - 1}, \tag{4}$$

$$\Theta_1 = \frac{1}{F}\left(1 - \sqrt{1 + 48F^2}\right) \quad \text{and} \quad \Theta_3 = \frac{1}{F}\left(1 + \sqrt{1 + 48F^2}\right). \tag{5}$$

The parameter "F" in Eq. (4) will reveal fundamental in characterizing the coupled lateral–torsional dynamic response behavior of eccentric systems. Careful examination of Eqs. (3a)–(3c), and of Fig. 2, which plots the normalized frequencies Ω_1, Ω_2 and Ω_3 as functions of "e" and "γ", reveals that Ω_1 is generally close to unity, while Ω_3 can be quite larger than one. Thus, it is found that in most practical cases, the first and second natural modes of vibration of the system have closely spaced frequencies, namely $\omega_1 \cong \omega_2 = \omega_L$. The following vibration mode shapes are also obtained as solution of the eigenvalue problem for undamped free vibration:[3]

$$\{\phi_1\} = \begin{bmatrix} \frac{e_y\sqrt{12}}{1-\Omega_1} \\ \frac{e_x\sqrt{12}}{\Omega_1-1} \\ 1 \end{bmatrix}, \quad \{\phi_2\} = \begin{bmatrix} e_x/e_y \\ 1 \\ 0 \end{bmatrix}, \quad \{\phi_3\} = \begin{bmatrix} \frac{e_y\sqrt{12}}{1-\Omega_3} \\ \frac{e_x\sqrt{12}}{\Omega_3-1} \\ 1 \end{bmatrix}. \tag{6}$$

[3]The analytical expressions for the mode shapes and natural frequencies given here apply only to laterally–torsionally coupled systems characterized by a non-zero eccentricity (i.e., $e = \sqrt{e_x^2 + e_y^2} \neq 0$). In the case of zero eccentricity, there are repeated eigenvalues and the degree of freedom $u_x(t), u_y(t)$ and $u_\theta(t)$ are already uncoupled.

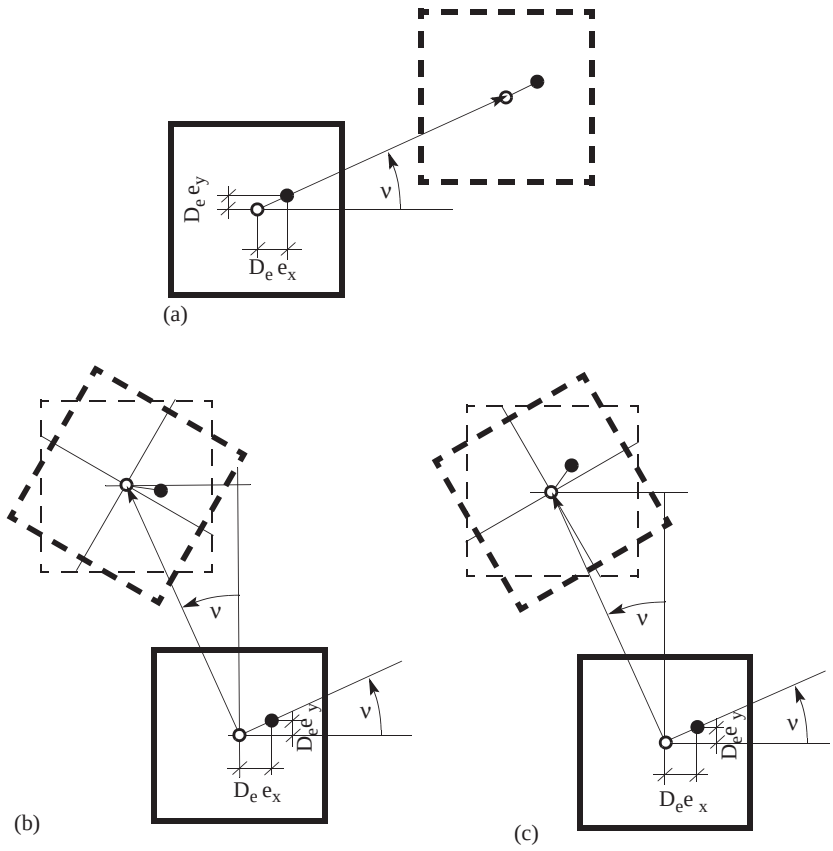

Fig. 3. Graphical representation of the mode shapes of the 3D one-story system with rigid in-plane diaphragm and non-coincident centers of mass and stiffness displayed in Fig. 1: (a) $\{\phi_2\}$, (b) $\{\phi_1\}$, (c) $\{\phi_3\}$; ● = center of stiffness, ○ = center of mass; $\nu = \arctan(e_y/e_x)$.

Careful examination of the analytical expressions for the three mode shapes in Eq. (6) shows that in the first and third modes, the translations are coupled with the rotation, while the second mode shape is purely translational in the direction defined by the center of mass and the center of stiffness. Fig. 3 provides a graphical representation of the mode shapes.

3. Undamped free vibration response

Undamped free vibrations of the eccentric system are governed by the set of coupled homogeneous differential equations given by Eq. (1) without the damping term, with zero right hand side and with the following initial conditions:

$$\begin{bmatrix} u_x(0) \\ u_y(0) \\ \rho u_\theta(0) \end{bmatrix} = \begin{bmatrix} 0 \\ a \\ 0 \end{bmatrix}, \tag{6a}$$

where "a" represents the initial deformation along the y-direction. Hereafter, the x- and y-axis are referred to as the transversal and longitudinal direction, respectively. The equations governing the free vibration response can be solved using the classical mode superposition method [29], which yields the following free vibration response histories along the original dofs:

$$u_y(t) = a\frac{e_x^2}{e^2}\left\{\frac{\Theta_3}{\Theta_3-\Theta_1}\cos(\omega_1 t) + \frac{e_y^2}{e_x^2}\cos(\omega_2 t) + \frac{\Theta_1}{\Theta_1-\Theta_3}\cos(\omega_3 t)\right\}, \tag{7a}$$

$$u_x(t) = a\frac{e_x e_y}{e^2}\left\{-\frac{\Theta_3}{\Theta_3-\Theta_1}\cos(\omega_1 t) + \cos(\omega_2 t) - \frac{\Theta_1}{\Theta_1-\Theta_3}\cos(\omega_3 t)\right\}, \tag{7b}$$

$$u_\theta(t) = \frac{a}{\sqrt{48}\rho}\frac{e_x}{e}\,\Theta_1\frac{\Theta_3}{\Theta_3-\Theta_1}\{\cos(\omega_1 t) - \cos(\omega_3 t)\}. \tag{7c}$$

Inspection of the expressions in Eqs. (7a)–(7c) leads to the following observations regarding the free vibration of eccentric systems induced by an initial displacement along the longitudinal (y-) direction:

- In the absence of longitudinal eccentricity ($e_y = 0$), the second mode of vibration is not excited in free vibration. On the other hand, both the first and third modes of vibration respond only if the system has a non-zero eccentricity "e_x" along the transversal (x-) direction.
- In order to have a non-zero free vibration response of the center of mass in the transversal (x-) direction, the structure must have eccentricities in both the x- and y- directions.
- In order to have free vibration displacement response histories with the same maximum amplitude in the longitudinal (y-) and transversal (x-) directions, it is necessary that $e_x = e_y$.[4]
- For a given transversal eccentricity "e_x", it can be shown that the system develops the largest rotational response when the longitudinal eccentricity is null ($e_y = 0$). This can be deduced from the factor $e_x/e(\Theta_1\Theta_3/(\Theta_3-\Theta_1)) = 24e_x/\sqrt{(\gamma^2-1)^2+48e^2}$ which controls the amplitude of the torsional response $u_\theta(t)$ in Eq. (7c).
- The longitudinal displacement, transversal displacement and rotational responses consist of the sum of trigonometric functions (harmonics) of various amplitudes and circular frequencies.

4. Fast and slow modes in free vibration response of undamped systems—beating phenomenon

To gain further insight into Eqs. (7a)–(7c), it is convenient to rewrite them as

$$u_y(t) = a\frac{e_x^2}{e^2}\left\{A_1\cos(\omega_1 t) + A_2\frac{e_y^2}{e_x^2}\cos(\omega_2 t) + A_3\cos(\omega_3 t)\right\}, \tag{8a}$$

$$u_x(t) = a\frac{e_x e_y}{e^2}\{-A_1\cos(\omega_1 t) + A_2\cos(\omega_2 t) - A_3\cos(\omega_3 t)\}, \tag{8b}$$

[4] $\frac{e_x e_y}{e_x^2+e_y^2} = \frac{1}{2} \Rightarrow (e_x - e_y)^2 = 0 \Rightarrow e_x = e_y$.

$$u_\theta(t) = \frac{a}{\rho}\frac{e_x}{e} A_4\{\cos(\omega_1 t) - \cos(\omega_3 t)\}, \tag{8c}$$

where

$$A_1 = \frac{1-\Omega_3}{\Omega_1-\Omega_3} = \frac{\Theta_3}{\Theta_3-\Theta_1} = \frac{\sqrt{1+48F^2}+1}{2\sqrt{1+48F^2}} = 1 - A_3, \tag{9a}$$

$$A_2 = 1, \tag{9b}$$

$$A_3 = \frac{\Omega_1-1}{\Omega_1-\Omega_3} = \frac{\Theta_1}{\Theta_1-\Theta_3} = \frac{\sqrt{1+48F^2}-1}{2\sqrt{1+48F^2}} = 1 - A_1, \tag{9c}$$

$$A_4 = \frac{1}{e\sqrt{12}}\frac{(\Omega_1-1)(\Omega_3-1)}{(\Omega_3-\Omega_1)} = \frac{1}{\sqrt{48}}\frac{\Theta_1\Theta_3}{\Theta_3-\Theta_1} = \sqrt{\frac{12F^2}{1+48F^2}}. \tag{9d}$$

It is worth mentioning the following properties of coefficients A_1 through A_4:

(a) $0.5 \leqslant A_1 \leqslant 1$ and, as shown in Fig. 4, for the most common values of "e" and "γ" parameters, A_1 lies in the range (0.72–0.90); (b) $0 \leqslant A_3 \leqslant 0.5$ and, as shown in Fig. 4, for the most common values of "e" and "γ" parameters, A_3 lies in the range (0.10–0.28); (c) $A_1 + A_3 = 1$; and (d) $0 \leqslant A_4 \leqslant 0.5$.

Analysis of Eqs. (8a)–(8c), in the light of the above remarks concerning the values of coefficients A_1, A_2 and A_3, leads to the following observations about the rotational, transversal and longitudinal components of the free vibration response of the system.

4.1. Rotational response $u_\theta(t)$

From Eq. (8c), the rotational response $u_\theta(t)$ is given by the sum of two harmonics of equal amplitude and well-separated circular frequencies ω_1 and ω_3. This results in a harmonic[5] (fast mode) with harmonically modulated (slow mode) amplitude or envelope. The fast mode has the circular frequency $\omega_{f\theta} = (\omega_1 + \omega_3)/2$ (also called sum frequency), while the slow mode has the circular frequency $\omega_{s\theta} = (\omega_1 - \omega_3)/2$ (also called difference frequency).

4.2. Transversal displacement response $u_x(t)$

From Eq. (8b), the transversal displacement response $u_x(t)$ is given as the sum of three harmonics. Two of them, of circular frequencies ω_1 and ω_2, have similar amplitudes ($A_2 = 1$ and A_1 is usually between 0.7 and 0.9), while the third one, of circular frequency ω_3, has an amplitude A_3 always smaller than 0.5 and most often in the range between 0. and 0.20. Neglecting this third harmonic (whose contribution to the total transversal motion can be seen as a small perturbation), the transversal displacement $u_x(t)$ can be approximated by the sum of two

[5] $\cos(\omega_1 t) + \cos(\omega_3 t) = 2\cos\left(\frac{\omega_1+\omega_3}{2}t\right)\cos\left(\frac{\omega_1-\omega_3}{2}t\right)$.

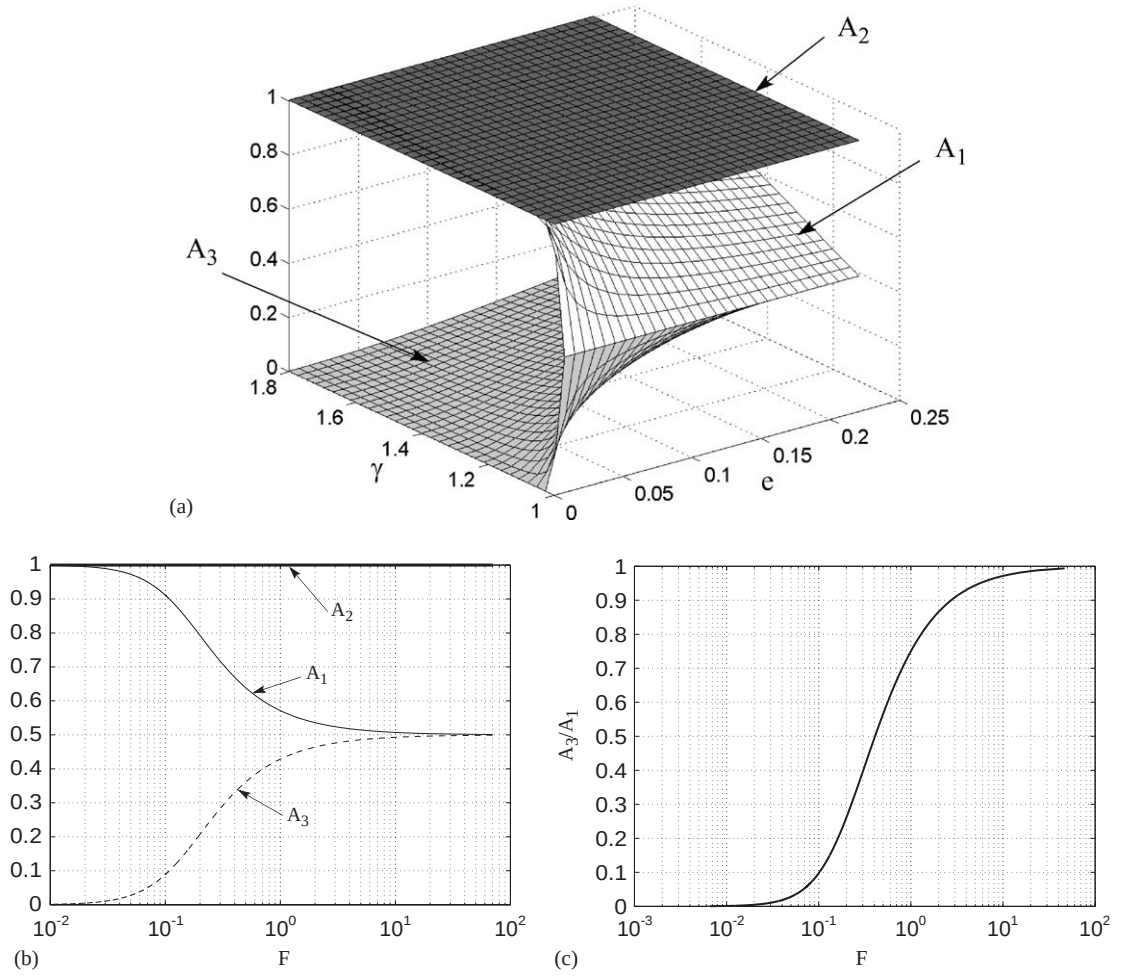

Fig. 4. Coefficients A_1, A_2, and A_3 (a) versus the "e" and "γ" parameters; (b) versus the "F" parameter; and (c) ratio A_3/A_1 versus "F".

harmonics of equal amplitude and circular frequencies ω_1 and ω_2. This results in a fast mode frequency $\omega_{fx} = (\omega_1 + \omega_2)/2$ and a slow mode frequency $\omega_{sx} = (\omega_1 - \omega_2)/2$.

4.3. Longitudinal displacement response $u_y(t)$

The algebraic expression for the longitudinal displacement response $u_y(t)$ in Eq. (8a) is similar to that for the transversal displacement response $u_x(t)$ in Eq. (8b). The main difference lies in the fact that the amplitude of the second harmonic (of circular frequency ω_2) is equal to $(e_y/e_x)^2$ in the case of $u_y(t)$ and to one in the case of $u_x(t)$. Thus, in the case of equal longitudinal and transversal eccentricities ($e_x = e_y$), the longitudinal and transversal displacement responses have the same frequencies of the fast and slow modes, i.e., $\omega_{fy} = \omega_{fx}$ and $\omega_{sy} = \omega_{sx}$. Further, in the case of null longitudinal eccentricity ($e_y = 0$), the longitudinal displacement response has the same fast and slow mode frequencies as the rotational displacement response, i.e., $\omega_{fy} = \omega_{f\theta}, \omega_{sy} = \omega_{s\theta}$.

4.4. Beating phenomenon

Fig. 5a shows the free vibration responses, $u_y(t), u_x(t)$ and $u_\theta(t)$, from an initial longitudinal displacement $a=0.10\,\text{m}$, of an eccentric system with parameters $e=0.1$, $\gamma=1.4$, and $\omega_L=\pi$ rad/s, for the special case of equal longitudinal and transversal eccentricities ($e_y=e_x$). It can be observed

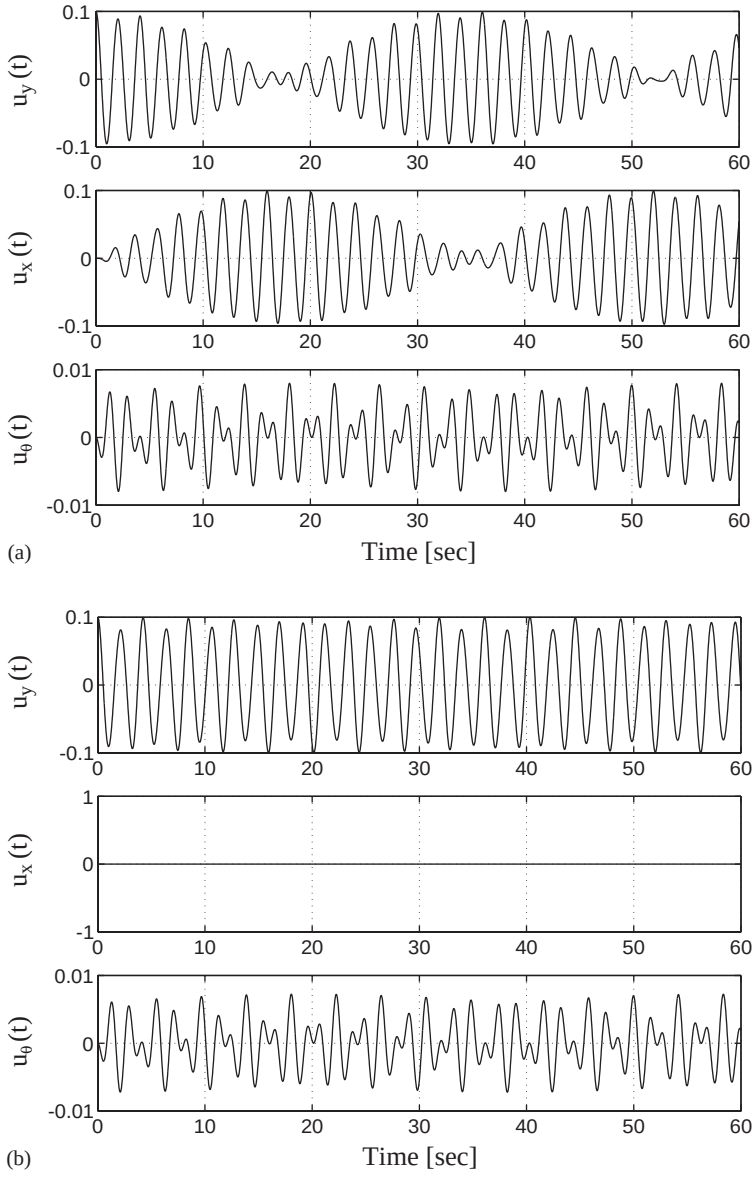

Fig. 5. Free vibration response ($u_y(t), u_x(t)$ and $u_\theta(t)$): (a) system characterized by $e_x=e_y, e=0.1, \gamma=1.4$, $\omega_L=\pi\,\text{rad/s}$, $D_e=28\,\text{m}$; (b) system characterized by $e_y=0, e_x=e=0.1, \gamma=1.2, \omega_L=\pi\,\text{rad/s}$, $D_e=28\,\text{m}$.

that: (a) the longitudinal and transversal displacements responses have a slow modulation of their amplitude due to the closeness of ω_1 and ω_2 given in Eqs. (3a) and (3c), while the rotational response exhibits a fast modulation of its amplitude due to the fact that ω_1 and ω_3 are well separated; (b) when the envelope of the longitudinal displacement reaches its maximum, that of the transversal displacement is at its minimum and vice versa, and (c) the rotational response has a high amplitude–modulation frequency due to the fact that ω_1 and ω_3 are well separated, which results in a strong interaction between the fast and the slow modes (due to the relative closeness of the fast and slow mode frequencies). Note that even though the initial displacement is imposed in the longitudinal (y-) direction, a longitudinal eccentricity (e_y) induces a mutual energy/motion transfer, which is maximized when $e_y = e_x$ (see footnote 4), between the longitudinal and transversal directions through the rotational response. As the parameter γ decreases, $(\omega_3 - \omega_1)$ increases and therefore the amplitude–modulation frequency of the responses $u_x(t)$ and $u_y(t)$ increases. Fig. 5b displays the free vibration response of a structure with the same parameters as the one in Fig. 5a, but for the special case of null longitudinal eccentricity ($e_y = 0$). Observe (a) the fast amplitude modulation of the rotational response $u_\theta(t)$ with interaction between fast and slow modes; (b) the null transversal response due to $e_y = 0$ according to Eq. (8b); and (c) the very limited amplitude modulation of the longitudinal response $u_y(t)$ due to the small value of the coefficient A_3 relative to the coefficient A_1 in Eq. (8a). Fig. 4c shows indeed that for most common values of "F" (i.e., between 0.10 and 0.30), the ratio A_3/A_1 lies in the range (0.10–0.40). Note that in this case a mutual energy/motion transfer occurs between the longitudinal and rotational responses.

5. Special case of zero longitudinal eccentricity

For the special case of zero longitudinal (y-direction) eccentricity ($e_y = 0$), which is of particular interest since for a given e_x it gives the maximum rotational response in free vibration initiated by a deformation along the y-direction, Eqs. (8a)–(8c) reduce to

$$u_y(t) = a\{A_1 \cos(\omega_1 t) + A_3 \cos(\omega_3 t)\}, \tag{10a}$$

$$u_x(t) = 0, \tag{10b}$$

$$u_\theta(t) = \frac{a}{\rho} A_4 \{\cos(\omega_1 t) - \cos(\omega_3 t)\}. \tag{10c}$$

5.1. Argand diagram representation of free vibration response

Fig. 6 shows the Argand diagram (or rotating vector) representation of the free vibration response given in Eqs. (10a) and (10c). The longitudinal displacement response, $u_y(t)$, is given by $\overrightarrow{OS'}$, the sum of the horizontal projections, $\overrightarrow{OC'}$ and $\overrightarrow{C'S'}$, of rotating vectors $\overrightarrow{OC}$, and $\overrightarrow{CS}$ of magnitude (aA_1) and (aA_3) and circular frequencies ω_1 and ω_3, respectively. The rotational

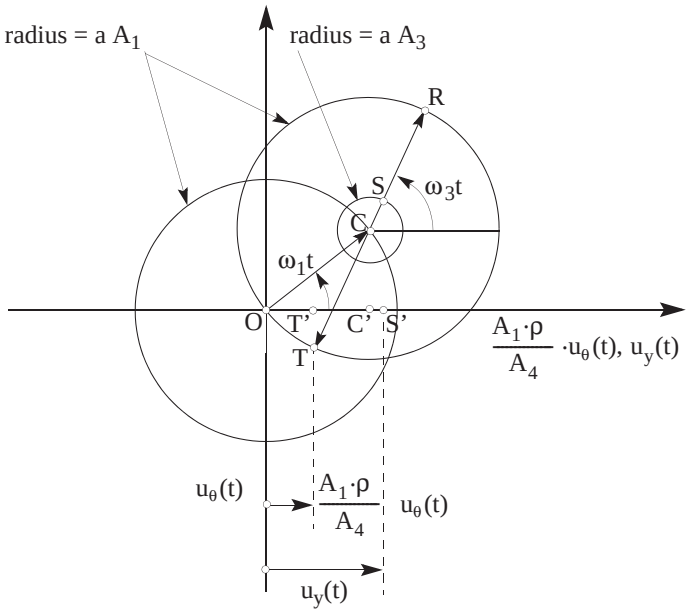

Fig. 6. Argand diagram or rotating vector representation of free vibration of undamped eccentric systems (Eqs. (10a) and (10c)).

response $u_\theta(t)$ is proportional to vector $\overrightarrow{OT'}$[6] which corresponds to the horizontal projection of the sum of rotating vectors $\overrightarrow{OC}$ and $\overrightarrow{CT}(=-\overrightarrow{CR})$. The fact that the radiuses $\overrightarrow{OC}$ and $\overrightarrow{CT}$ have equal length $(=aA_1)$, while the radius $\overrightarrow{CS}(=aA_3)$ is generally quite smaller (see Fig. 4c) leads to the following observations regarding free vibration of laterally–torsionally coupled systems from an initial longitudinal displacement a:

(a) The maximum longitudinal displacement magnitude, $|u_y|_{\max}=a(A_1+A_3)=a$, is developed for $\omega_1 t=n\pi$ and $\omega_3 t=m\pi$ (with n and m both odd or both even), and for these conditions the rotational response $u_\theta(t)$ is always zero. However, due to the small value of A_3 relative to A_1, when $\omega_1 t\cong n\pi$, the longitudinal displacement response $u_y(t)$ is close to its maximum value. More precisely, when $\omega_1 t=n\pi$, we have that $a\leqslant|u_y(t)|\leqslant a(A_1-A_3)$.

(b) The maximum rotational response is developed when $\omega_1 t=n\pi$ and $\omega_3 t=(m+1)\pi$, with n and m both even or odd. In these conditions, the longitudinal displacement magnitude is equal to "$a(A_1-A_3)$", and is therefore close to $|u_y|_{\max}$ for small values of A_3 (which are common). Thus, it is possible to state that, for structures with small values of A_3, rotational and longitudinal displacement responses are close to their maxima at the same time. This is a fundamental observation that will be used in the development of the simplified analysis procedure presented in Sections 7–9.

[6] $u_\theta(t)=\dfrac{\Theta_1}{\rho\sqrt{48}}\overrightarrow{OT'}=\dfrac{A_4}{A_1\rho}\overrightarrow{OT'}$.

(c) When $\omega_1 t = \pi/2 + n\pi$, the magnitude of the longitudinal displacement response is bounded by (aA_3).
(d) Considering the special case in which $\omega_1 t = \pi/2 \pm \arcsin(A_3/A_1) + n\pi$, it is possible to state that, when the longitudinal displacement response is zero, the magnitude of the rotational response is bounded by $\frac{1}{2}|u_\theta|_{\max}(1 + A_3/A_1)$. Given the small value of the ratio A_3/A_1 (see Fig. 4c), this bound approximates to $\frac{1}{2}|u_\theta|_{\max}$.

5.2. Fast and slow modes

Eq. (10a) shows that, due to the relatively small value of A_3/A_1, the longitudinal displacement response $u_y(t)$ is well approximated by a single harmonic of circular frequency ω_1. On the other hand, the rotational response $u_\theta(t)$ is a harmonic motion with harmonically modulated amplitude and slow mode circular frequency $\omega_{s\theta} = (\omega_3 - \omega_1)/2$. Noting that the slow mode of a beating phenomenon reaches its maximum (i.e., envelope maximum) twice during one period of the slow mode, it follows that the time necessary for the slow mode of the rotational response to develop a full modulation of the response amplitude is $\frac{1}{2}T_{s\theta} = \pi/\omega_{s\theta}$. Therefore, the number of longitudinal (y-) response cycles necessary to develop a full modulation of the rotational response amplitude is approximately equal to

$$\frac{1}{2}\frac{T_{s\theta}}{T_1} = \frac{1}{2}\frac{\omega_1}{\omega_{s\theta}} = \frac{\omega_1}{\omega_3 - \omega_1} = \left(1 - \sqrt{\frac{\Omega_3}{\Omega_1}}\right)^{-1}, \tag{11}$$

where $T_1 = 2\pi/\omega_1$ denotes the approximated period of the longitudinal response $u_y(t)$ and Ω_1 and Ω_3 are defined in Eqs. (3a) and (3c), respectively.

Fig. 7 plots the exact closed-form solution for $T_{s\theta}/2T_1$ and indicates that, for most values of "e" and "γ" parameters considered here, only about one cycle of longitudinal response is necessary to develop a full modulation of the rotational response amplitude. Only for a restricted range of the "e" and "γ" parameters, namely for small values of "e" and "γ", the number of longitudinal cycles necessary to develop a full modulation of the rotational response amplitude reaches values of about 4. Thus, the free vibration rotational response of undamped most common eccentric systems is characterized by a fast modulation of its amplitude resulting in a strong interaction between the fast and slow modes.

Figs. 8a and b show the history of the rotational response $u_\theta(t)$ versus the longitudinal displacement response $u_y(t)$ of an undamped eccentric system in free vibration (from an initial displacement $a = 0.1$ m along the y-direction) for the special case of zero longitudinal eccentricity ($e_y = 0$). Careful examination of these plots reveals that for every longitudinal cycle of vibration, the rotational response reaches a value close to its maximum, $|u_\theta|_{\max}$, at an instant when the longitudinal displacement response is close but not equal to its maximum, $|u_y|_{\max}$. It can also be observed that, as predicted by the Argand diagram representation of the response in previous section, (a) when the maximum longitudinal displacement response is developed, the rotational response is zero, (b) when the maximum rotational response is developed, the longitudinal displacement response is equal to[7] $|u_y|_{\max}(1 - 2A_3)$ where $|u_y|_{\max} = a = 0.1$ m, and (c) when the longitudinal displacement is zero, the rotational response is smaller or equal to $\frac{1}{2}|u_\theta|_{\max}(1 + A_3/A_1)$.

[7]This longitudinal displacement response, due to the small value of A_3, is close to $|u_y|_{\max}$.

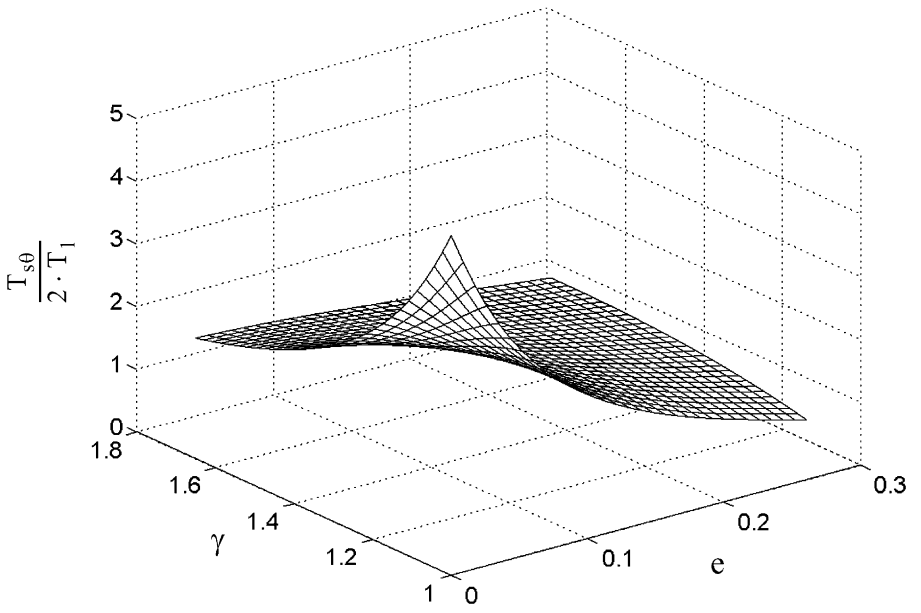

Fig. 7. $T_{s\theta}/(2T_1)$ as a function of parameters "e' and "γ".

6. Damped free vibration response

The free vibration response histories of classically damped eccentric systems (from a given initial displacement "a" along the y-direction and assuming equal[8] viscous damping ratios, i.e., $\xi_1 = \xi_2 = \xi_3 = \xi$) are given by

$$u_y(t) = a\frac{e_x^2}{e^2}\Lambda \operatorname{Exp}(-\xi\omega_1 t)\Big\{A_1 \cos(\omega_{D1}t + \theta) + A_2 \operatorname{Exp}(-\xi(\omega_2 - \omega_1)t)\frac{e_y^2}{e_x^2}\cos(\omega_{D2}t + \theta) + A_3 \operatorname{Exp}(-\xi(\omega_3 - \omega_1)t)\cos(\omega_{D3}t + \theta)\Big\}, \tag{12a}$$

$$u_x(t) = a\frac{e_x e_y}{e^2}\Lambda \operatorname{Exp}(-\xi\omega_1 t)\{-A_1 \cos(\omega_{D1}t + \theta) + A_2 \operatorname{Exp}(-\xi(\omega_2 - \omega_1)t)\cos(\omega_{D2}t + \theta) - A_3 \operatorname{Exp}(-\xi(\omega_3 - \omega_1)t)\cos(\omega_{D3}t + \theta)\}, \tag{12b}$$

$$u_\theta(t) = \frac{a}{\rho}\frac{e_x}{e}A_4\Lambda \operatorname{Exp}(-\xi\omega_1 t)\{\cos(\omega_{D1}t + \theta) - \operatorname{Exp}(-\xi(\omega_3 - \omega_1)t)\cos(\omega_{D3}t + \theta)\}, \tag{12c}$$

where $\omega_{Di} = \omega_i\sqrt{1-\xi^2}, i = 1,2,3$, are the modal damped natural circular frequencies;

$$\Lambda = \left(1 + \frac{\xi}{\sqrt{1-\xi^2}}\right)^{1/2} \quad \text{and} \quad \theta = -\operatorname{atan}\left(\frac{\xi}{\sqrt{1-\xi^2}}\right), \quad i = 1,2,3.$$

[8]For base isolated structures, as all three modes involve deformations of resisting elements (base isolators) having in general similar characteristics, the assumption of equal effective modal damping ratios is reasonable.

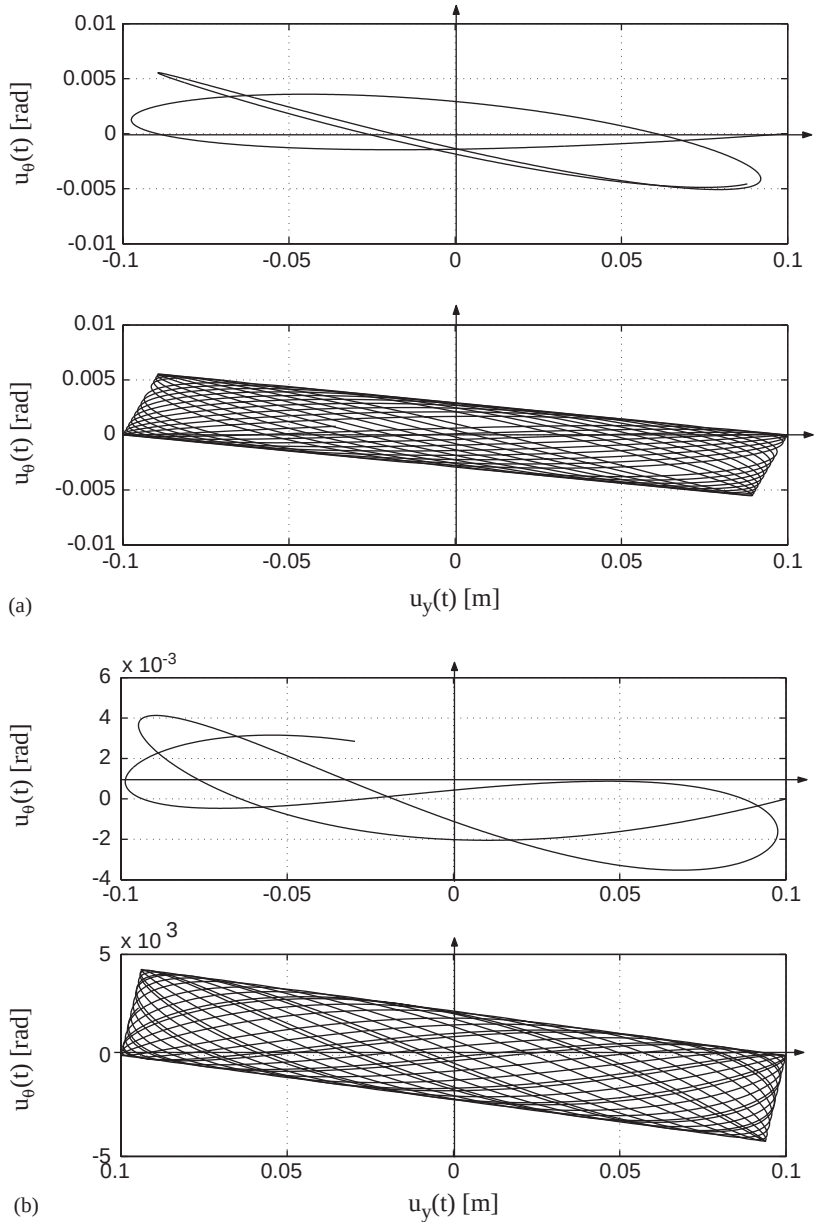

Fig. 8. Time evolution of u_θ versus u_y (Eqs. (7a) and (7c)) for an undamped eccentric structure characterized by $e_y = 0, D_e = 28\,\text{m}, \omega_L = \pi\,\text{rad/s}$ and $a = 0.1\,\text{m}$: (a) $\gamma = 1.3, e_x = 0.05$; (b) $\gamma = 1.7, e_x = 0.1$.

Note that for zero modal damping ratios ($\xi = 0$), $\Lambda = 1$ and $\theta = 0$, Eqs. (12a)–(12c) reduce to Eqs. (8a)–(8c), respectively. Also note that Eqs. (12a)–(12c) are very similar to the corresponding Eqs. (8a)–(8c) for undamped systems, the main difference being: (a) an overall response decay in time, and (b) a relative amplitude decay in time of the harmonics at frequencies ω_{D2} and ω_{D3} with

respect to the amplitude of the harmonic at frequency ω_{D1}. This relative amplitude decay is larger for the ω_{D3} harmonic than for the ω_{D2} harmonic.

The observed similar structure of the governing equations of motion for both undamped and damped eccentric systems and response history simulation studies indicate that damped and undamped eccentric systems in free vibration follow similar behavioral patterns. Fig. 9 compares the damped (assuming $\xi = 5\%$) and undamped free vibration responses in the "$u_y - u_\theta$" space of two eccentric structures of parameter $\gamma = 1.3$ and $\gamma = 1.7$, respectively, for the special case of zero longitudinal eccentricity ($e_y = 0$). Note that the damping-induced reduction (as compared to the undamped case) of the maximum rotational response developed in the first few cycles is larger for the system with the smaller parameter γ. This is due to the fact that, as shown in Section 5.2, for structures characterized by small (close to one) values of the γ parameter, it takes a relatively larger number of longitudinal oscillations to develop the maximum rotational response amplitude $|u_\theta|_{\max}$.

Fig. 10a shows the Argand diagram representation of the free vibration response [Eqs. (12a)–(12c)] of a damped eccentric system for the special case $e_y = 0$. Note that in the damped case, the amplitude of the three rotating vectors decays exponentially in time, but with faster relative decay for the two vectors rotating at frequency ω_{D3}. As a result, for the damped case, an even stronger correlation exists between the longitudinal and rotational responses as compared to the undamped case.

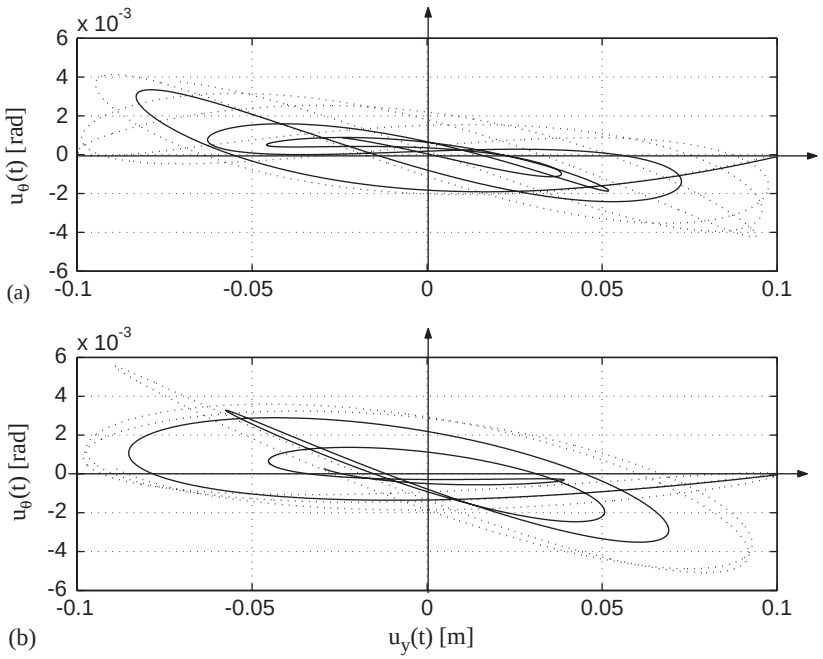

Fig. 9. Time evolution of u_θ versus u_y for an undamped structure (Eqs. (7a) and (7c)—dotted line) and a 5% damped structure (Eqs. (12a) and (12c)—solid line), both characterized by $e_y = 0, D_e = 28\,\text{m}, \omega_L = \pi$ [rad/s], and $a = 0.1\,\text{m}$: (a) $\gamma = 1.7, e_x = 0.1$; (b) $\gamma = 1.3, e_x = 0.05$.

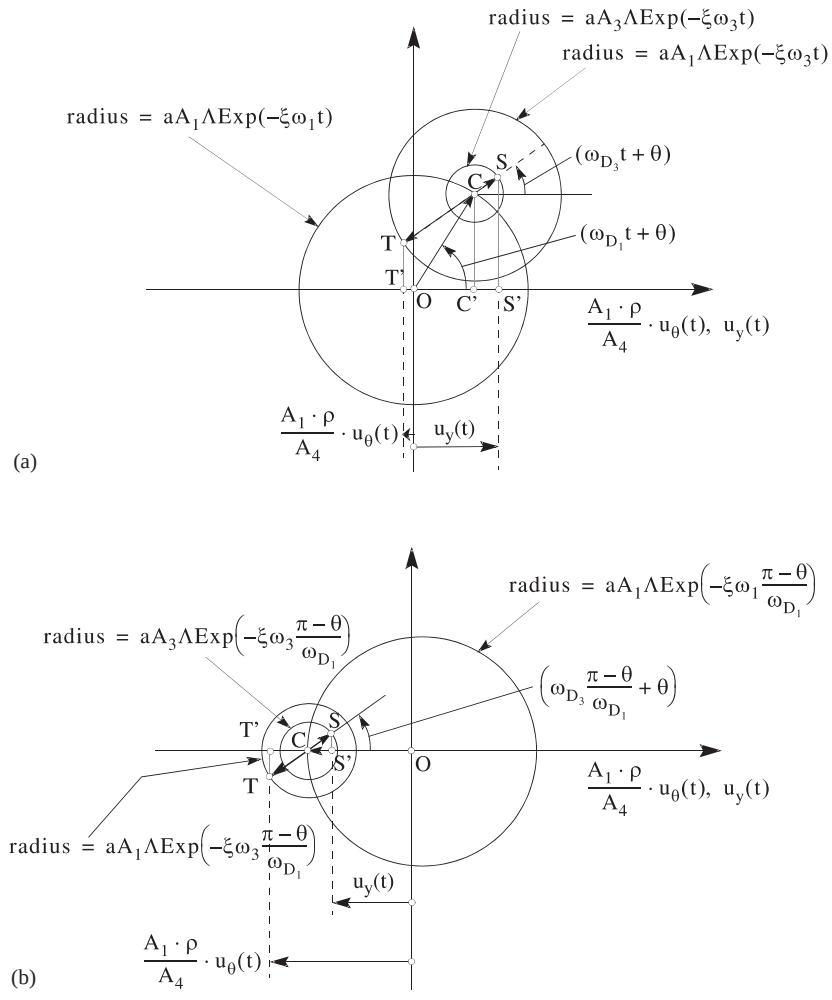

Fig. 10. Argand diagram (rotating vector) representation of free vibration of damped eccentric systems (Eqs. (12a) and (12c)), for the special case of null longitudinal eccentricity ($e_y = 0$): (a) general representation; (b) representation at $t = (\pi - \theta)/\omega_{D_1}$ s.

Fig. 10(b) shows the Argand diagram representation of the longitudinal and rotational free vibration responses of a damped eccentric system with zero longitudinal eccentricity at time $t = (\pi - \theta)/\omega_{D1}$. At this instant of time, it is seen that the response quantities $u_y(t)$ and $(A_1\rho/A_4)u_\theta(t)$ are closer than in the corresponding situation (i.e., at $t = \pi/\omega_1$) without damping.

7. Maximum rotational to maximum longitudinal displacement response ratio of undamped and damped eccentric systems in free vibration

In the previous sections, it was shown that eccentric systems (in the special case of zero longitudinal eccentricity) develop, almost simultaneously and almost once per longitudinal

oscillation, a rotational and longitudinal response close to their respective maxima. This behavior suggested that the maximum rotational and maximum longitudinal displacement responses of eccentric systems might be strongly correlated, their ratio representing a basic property of eccentric systems, which controls their dynamic response also under general forced vibration conditions. On this basis, the ratio of the maximum rotational to maximum longitudinal displacement response, $(|u_\theta|_{\max}/|u_y|_{\max})_{fv}$, developed by eccentric structures in free vibration from a given initial longitudinal displacement "a" is investigated below for the special case of zero longitudinal eccentricity.[9]

For undamped eccentric structures, the ratio $(|u_\theta|_{\max}/|u_y|_{\max})_{fv,u}$ can be expressed in closed-form from Eqs. (7a) and (7c) as

$$\left(\frac{|u_\theta|_{\max}}{|u_y|_{\max}}\right)_{fv,u} = \frac{4e\sqrt{3}}{\rho\sqrt{(\gamma^2-1)^2+48e^2}} = \frac{1}{\rho}\frac{\sqrt{48F^2}}{\sqrt{48F^2+1}}. \tag{13}$$

Eq. (13) shows that $(|u_\theta|_{\max}/|u_y|_{\max})_{fv,u}$ is inversely proportional to the mass radius of gyration ρ of the structure; thus suggesting the following dimensionless rotational parameter:

$$\alpha_u = \rho\left(\frac{|u_\theta|_{\max}}{|u_y|_{\max}}\right)_{fv,u} = \frac{4e\sqrt{3}}{\sqrt{(\gamma^2-1)^2+48e^2}} = \frac{\sqrt{48F^2}}{\sqrt{48F^2+1}}. \tag{14}$$

From the graphical representation of the above rotational parameter α_u given in Fig. 11, it is observed that for the same initial longitudinal displacement, eccentric systems can develop very different values of maximum rotational response depending on the system characteristics. Eq. (14) and Fig. 11 indicate that the rotational parameter is bounded between zero and one ($0 \leqslant \alpha_u \leqslant 1$), thus limiting the maximum rotational response $|u_\theta|_{\max}$ that can be developed in free vibration by any eccentric linear elastic system to

$$|u_\theta|_{\max} \leqslant \frac{|u_y|_{\max}}{\rho} = \frac{a}{\rho} = \frac{\sqrt{12}|u_y|_{\max}}{D_e}. \tag{15}$$

This is a fundamental result. Note also that for $\gamma = 1$, the maximum rotational response reaches this upper bound independently of the eccentricity "e". The rotational parameter α_u depends on the pair of system parameters "e" and "γ" or, even better, on the single structural parameter $F = e/(\gamma^2-1)$.

Due to the exponential decay in time of the amplitude of the various harmonic components of the damped free vibration response in Eqs. (12a) and (12c), unlike in the undamped case it is not possible to obtain a simple exact closed-form expression for the maximum rotational to maximum

[9] In the case $e_y \neq 0$, the value of the ratio is given by

$$\left(\frac{|u_\theta|_{\max}}{|u_y|_{\max}}\right)_{fv,u} = \frac{1}{\rho}\frac{e_x}{e}\frac{\sqrt{48F^2}}{\sqrt{48F^2+1}}.$$

Recall that for a given eccentricity e_x, the largest maximum rotational response is obtained for $e_y = 0$ as shown in Section 4.

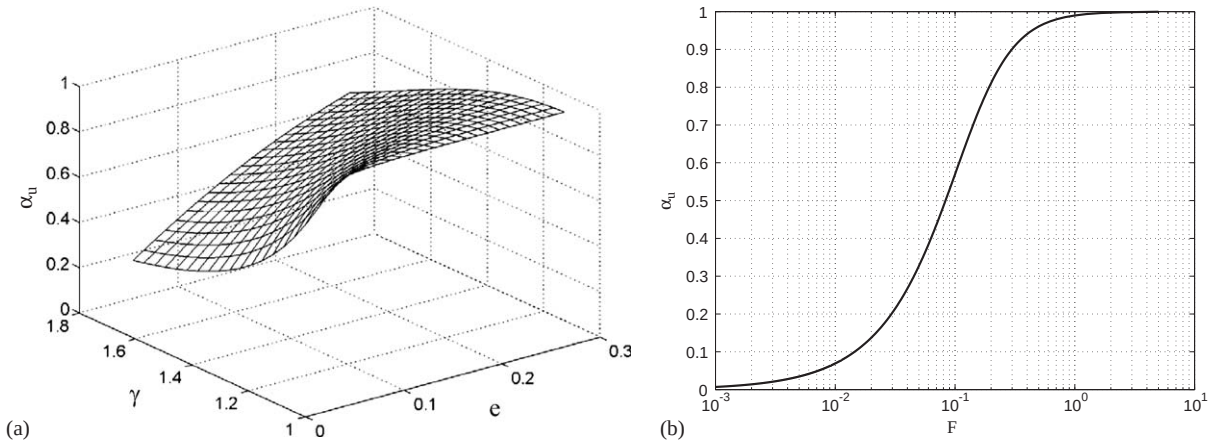

Fig. 11. "Alpha" parameter α_u: (a) as a function of "e" and "γ"; (b) as a function of "F".

longitudinal displacement ratio. However, an upper bound analysis yields the following result:

$$\alpha_d = \rho\left(\frac{|u_\theta|_{\max}}{|u_y|_{\max}}\right)_{fv,d} \leqslant \Lambda\frac{1}{2}\,\alpha_u\,\mathrm{Max}\left\{1, \mathrm{Exp}\left(-\xi\frac{\pi}{2}\sqrt{\frac{\Omega_1}{\Omega_3}}\right) + \mathrm{Exp}\left(-\xi\frac{\pi}{2}\right)\right\}. \tag{16}$$

For the ranges of parameters considered in this study ($0.02 \leqslant e \leqslant 0.22, 1.05 \leqslant \gamma \leqslant 1.80$), the above upper bound is governed by the second argument of the Max() function for values of modal damping ratio up to 0.30. Note also that for zero damping the above upper bound reduces to α_u, the analytically exact value of $\rho(|u_\theta|_{\max}/|u_y|_{\max})_{fv,u}$ for undamped free vibration. Due to the lack of an exact analytical expression for the rotational parameter α_d, this ratio was obtained, for the special case of $e_y = 0$, through extensive numerical simulations carried over a wide range of system parameter values, namely $0.02 \leqslant e \leqslant 0.22$, $1.05 \leqslant \gamma \leqslant 1.80$, and $0.02 \leqslant \xi \leqslant 0.12$. The following empirical analytical expressions were obtained for α_d through least-squares fitting:

$$\alpha_d = -1.74e + 15.71\frac{e}{\gamma^2} - 51.17\frac{e^2}{\gamma^4}, \quad \xi = 2\%, \tag{17a}$$

$$\alpha_d = -1.11e + 12.55\frac{e}{\gamma^2} - 39.18\frac{e^2}{\gamma^4}, \quad \xi = 4\%, \tag{17b}$$

$$\alpha_d = -0.88e + 11.30\frac{e}{\gamma^2} - 34.58\frac{e^2}{\gamma^4}, \quad \xi = 5\%, \tag{17c}$$

$$\alpha_d = -0.70e + 10.25\frac{e}{\gamma^2} - 30.70\frac{e^2}{\gamma^4}, \quad \xi = 6\%, \tag{17d}$$

$$\alpha_d = -0.46e + 8.64\frac{e}{\gamma^2} - 24.95\frac{e^2}{\gamma^4}, \quad \xi = 8\%, \tag{17e}$$

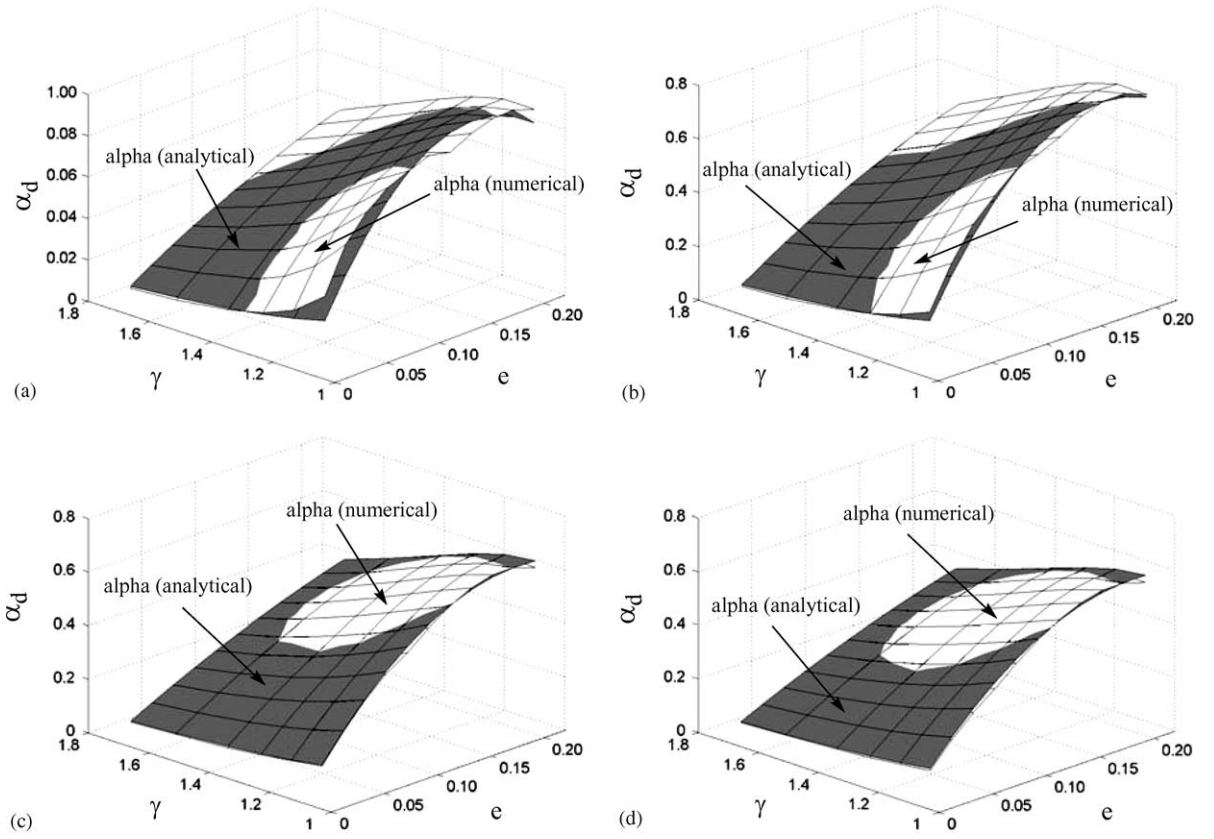

Fig. 12. Values of the alpha parameter α_d given by Eqs. (16) (approximate analytical solution) compared with the corresponding values obtained through numerical simulation: (a) $\xi = 2\%$; (b) $\xi = 5\%$; (c) $\xi = 10\%$; (d) $\xi = 12\%$.

$$\alpha_d = -0.31e + 7.45\frac{e}{\gamma^2} - 20.95\frac{e^2}{\gamma^4}, \quad \xi = 10\%, \tag{17f}$$

$$\alpha_d = -0.23e + 6.59\frac{e}{\gamma^2} - 18.19\frac{e^2}{\gamma^4}, \quad \xi = 12\%. \tag{17g}$$

Fig. 12 compares the values of α_d provided by Eq. (16) with the numerically simulated values of α_d and indicates a good fit due to the smoothness of function $\alpha_d(e, \gamma)$.

8. Maximum rotational to maximum longitudinal displacement response ratio for undamped and damped eccentric systems in forced vibration

The study of the free vibration of eccentric systems has shown that the ratio of the maximum rotational to the maximum longitudinal displacement response has a smooth but strong dependence on only a few system parameters. These interesting results suggested to investigate the

values taken by this response ratio under forced vibration conditions. Extensive numerical earthquake response simulations were performed for eccentric systems over a wide range of system parameters, namely $0.02 \leqslant e \leqslant 0.24, 1.05 \leqslant \gamma \leqslant 1.80, 0.02 \leqslant \xi \leqslant 0.15$, and using a set of 125 historical ground motion records (20 of which are near-field records defined by a site-to-source distance smaller than 10 km) as earthquake forcing functions. These records include the El Centro record (N–S comp.) of the 1940 Imperial Valley earthquake, the Taft record (E–W comp.) of the 1952 Kern County earthquake, the Cholame record (E–W comp.) of the 1966 Parkfield earthquake, the Lucern record (E–W comp.) of the 1992 Landers Earthquake, the Rancho Palos Verdes record (N–S comp.) of the 1994 Northridge earthquake, and the Oka record (N–S comp.) of the Kobe 1995 earthquake. As in the analyses performed in the previous section, the systems here analyzed are characterized by a null longitudinal eccentricity ($e_y = 0$) and an excitation applied in the longitudinal (y-) direction. The results obtained show that the response ratio $\rho|u_\theta|_{\max}/|u_y|_{\max}$ for earthquake excitation remains close to its counterpart for damped free vibration, i.e.,

$$\left(\rho \frac{|u_\theta|_{\max}}{|u_y|_{\max}}\right)_{\text{eqke}} \cong \alpha_d. \tag{18}$$

Fig. 13 shows the results obtained for eccentric structures with 4% modal damping ratios and parameter $\gamma = 1.18, 1.41, 1.73$. This figure compares the mean value and the mean ± one standard deviation of the response ratio $\rho|u_\theta|_{\max}/|u_y|_{\max}$ over the selected set of 125 earthquake ground motions with the corresponding rotational response parameters α_u and α_d under free vibration conditions. It is seen that the mean value of the response ratio is relatively close to α_d. It is also observed that the rotational parameter α_u, available in closed-form from Eq. (14) and function of parameter "F" only defined in Eq. (5), appears to provide a good upper bound for the response ratio $\rho|u_\theta|_{\max}/|u_y|_{\max}$ induced by earthquake excitation. The following small differences were obtained between the results for the far- and near-field records, respectively: the mean value of the response ratio $\rho|u_\theta|_{\max}/|u_y|_{\max}$ is about 15%, 8%, and 0% larger for the near-field records than for the far-field records for $\gamma = 1.18, 1.41$, and 1.73, respectively.

Also, numerical dynamic simulations were performed for eccentric systems subjected to a sum of two harmonic excitations

$$p_y(t) = A_L \cos(\omega_L t) + A_\theta \cos(\omega_\theta t). \tag{19}$$

A representative set of the results obtained is given in Fig. 14. It is observed that for $A_L/A_\theta = 1$, the response ratio $\rho|u_\theta|_{\max}/|u_y|_{\max}$ almost coincides with the rotational parameter α_d. Also in this case, parameter α_u represents an upper bound for the response ratio $\rho|u_\theta|_{\max}/|u_y|_{\max}$.

9. Alpha-method for prediction of maximum rotational response of eccentric systems

The results presented in previous sections strongly indicate that the response ratio $\rho|u_\theta|_{\max}/|u_y|_{\max}$ is a robust, low-variability response parameter, which is only weakly excitation dependent and therefore strongly system dependent. This fundamental property forms the basis of the proposed simplified analysis procedure presented in this section. Hereafter, the dimensionless response ratio $\rho|u_\theta|_{\max}/|u_y|_{\max}$ obtained for free vibration conditions and termed α_u and α_d for

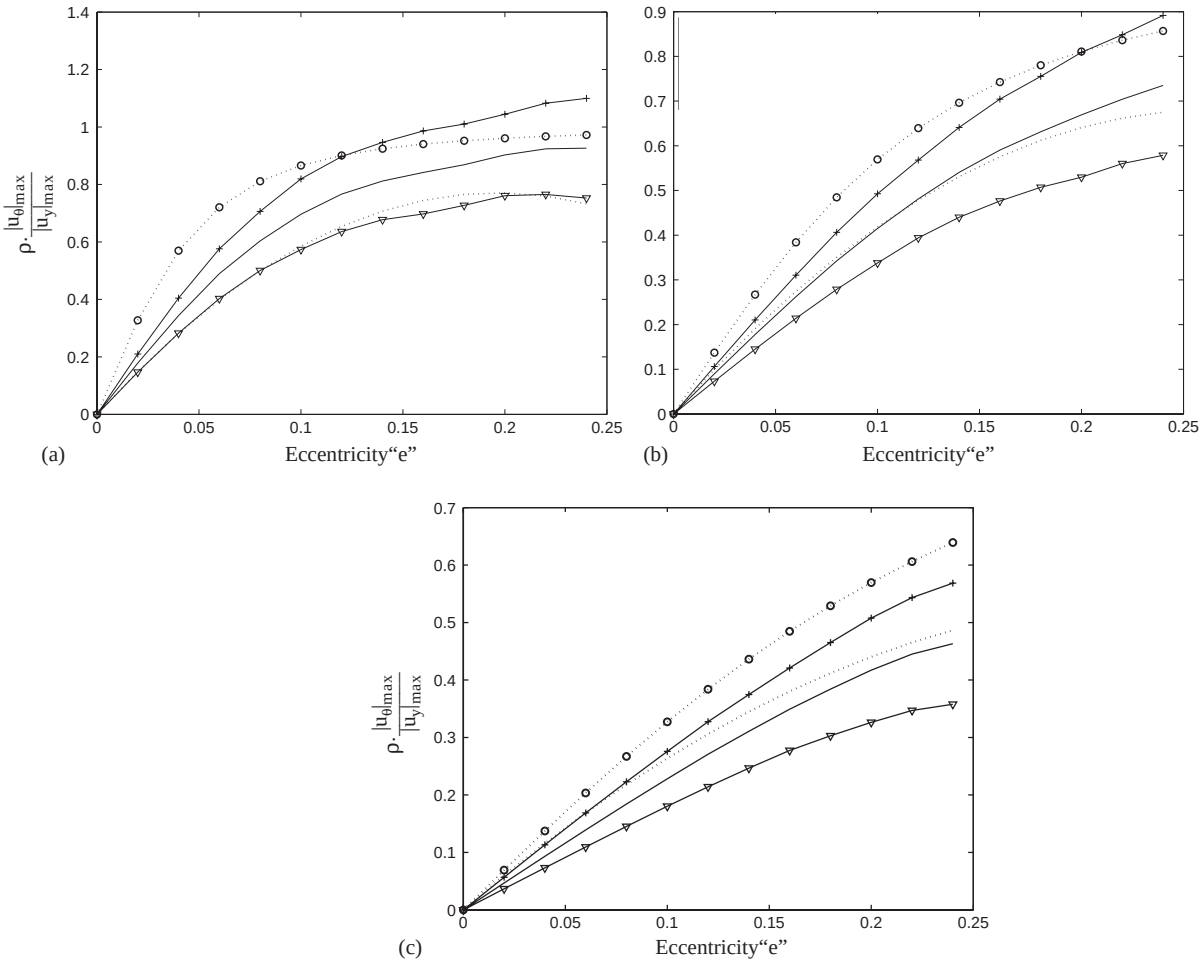

Fig. 13. Values of $\rho|u_\theta|_{\max}/|u_y|_{\max}$ as a function of the relative eccentricity "e" obtained from earthquake response simulations based on a set of 125 historical earthquake input records (all structures are characterized by $\xi = 4\%$): (a) $\gamma = 1.18$; (b) $\gamma = 1.41$; (c) $\gamma = 1.73$; —, mean; —+—, mean + one s.d.; —▽—, mean − one s.d.; - -○- -, alpha (undamped); - - - - -, alpha (damping = 4%).

undamped and damped eccentric systems, respectively, will be referred to as the "α" parameter. Structures characterized by large values of "α" have a predisposition for developing large rotational response.

The limited difference between "α" and the corresponding value of the ratio $\rho|u_\theta|_{\max}/|u_y|_{\max}$ developed under forced vibration conditions suggests the following simple relationship between $|u_\theta|_{\max}$ and $|u_y|_{\max}$:

$$|u_\theta|_{\max} \cong \alpha \frac{|u_y|_{\max}}{\rho}. \tag{20}$$

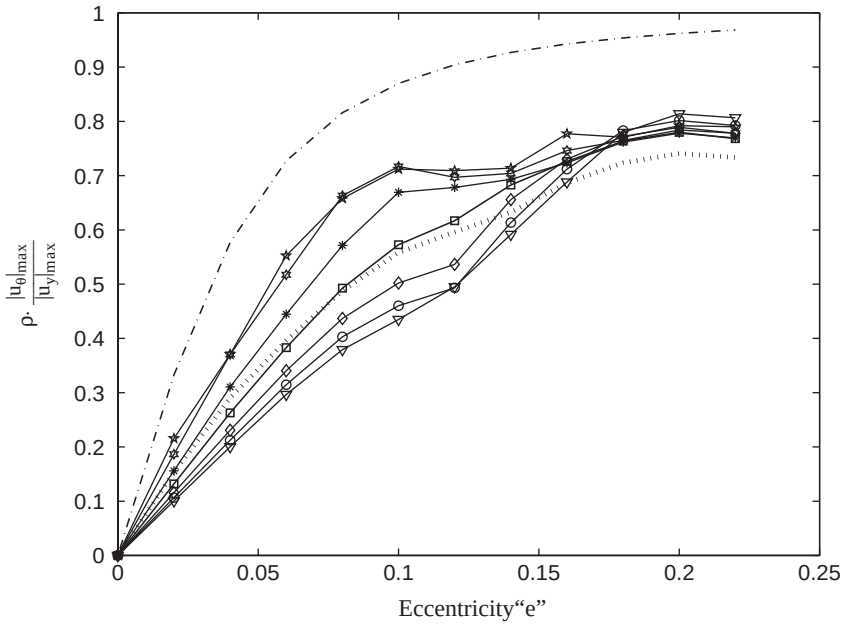

Fig. 14. Response parameter $\rho|u_\theta|_{\max}/|u_y|_{\max}$ versus "e" for eccentric structures subjected to the driving force defined in Eq. (19): $\gamma = 1.18$, $\xi = 4\%$; —▽—, $A_L/A_\theta = 10$; —○—, $A_L/A_\theta = 4$; —◇—, $A_L/A_\theta = 2$; —□—, $A_L/A_\theta = 1$; —✻—, $A_L/A_\theta = \frac{1}{2}$; —✡—, $A_L/A_\theta = \frac{1}{4}$; —★—, $A_L/A_\theta = \frac{1}{10}$; —·—, α_u (alpha undamped); - - - - -, α_d (alpha damped).

Other research work [23,24] shows that the maximum longitudinal displacement response, $|u_y|_{\max}$, of an eccentric structure does not differ significantly from the maximum longitudinal displacement, $|u_y|_{\max-\mathrm{ne}}$, developed by a structure having equivalent dynamic characteristics, but with no eccentricity. As an illustration of this fact, selected numerical results are plotted in Fig. 15 (for $e_y = 0$ and $\gamma = 1.18$) showing that for increasing values of eccentricity "e", the maximum longitudinal displacement response does not change significantly. Thus,

$$|u_y|_{\max} \cong |u_y|_{\max-\mathrm{ne}} \tag{21}$$

which, when used in conjunction with Eq. (20) yields the following formula for maximum rotational response prediction:

$$|u_\theta|_{\max} \cong \alpha \frac{|u_y|_{\max-\mathrm{ne}}}{\rho}. \tag{22}$$

Eq. (22), provides a powerful tool for simplified (code-like) analysis of the torsional response of eccentric structures. The maximum longitudinal displacement response of the equivalent non-eccentric structure, $|u_y|_{\max-\mathrm{ne}}$, is readily obtained as the maximum deformation of an sdof oscillator of undamped natural period $T_L = 2(\pi)/\omega_L$, damping ratio ξ, and mass equal to the total mass of the structure (e.g., response spectrum [29]).

Base isolated structures represent one of the main applications of the proposed "α" method for simplified analysis of 3-dof laterally–torsionally coupled systems. For these structures,

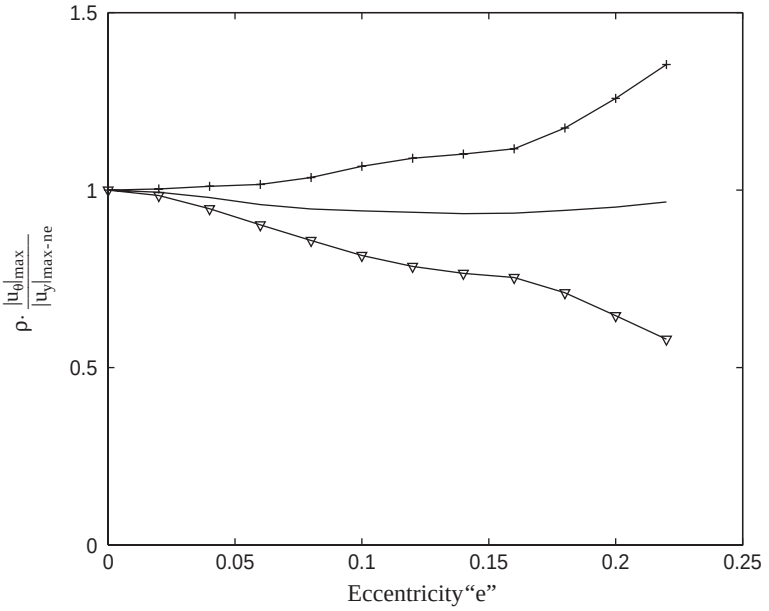

Fig. 15. Eccentric to non-eccentric maximum longitudinal displacement ratio, $|u_{y,\max}|/|u_{y,\max\,-\mathrm{ne}}|$, as a function of the relative eccentricity "e" obtained from earthquake response simulations based on a set of 100 historical earthquake input records: $\gamma = 1.18$, $\xi = 4\%$; —, mean; —+—, mean + one s.d.; —▽—, mean − one s.d.

determination of the maximum isolator deformation is a key design parameter. It is useful to note that for rectangular base-isolated structures, $\alpha\sqrt{3}$ represents the ratio of the displacement at the corner of the structure (along the direction orthogonal to the diagonal) caused by the maximum rotational response, $|u_{\theta,\max}|$, to the maximum longitudinal displacement response at the center of mass of the structure, $|u_{y,\max}|$, as shown in Fig. 16. This observation provides a clear geometric interpretation of the parameter "α". A fundamental result presented in Section 8 is that parameter "α" is bounded by one from above. It follows that the maximum corner displacement (along the direction orthogonal to the diagonal) caused by the maximum rotational response is bounded by $\sqrt{3}|u_{y,\max}| = 1.73|u_{y,\max}|$.

10. Comparison between IBC provisions and proposed "alpha" method

According to the provisions of the International Building Code (IBC) (formerly Uniform Building Code (UBC)) and the Structural Engineers Association of California [6,31,32], the total maximum design displacement of the isolators D_{TM} (including torsional effects) can be estimated as (Eqs. (16–83) and (16–84) of IBC)

$$D_{TM} = D_M\left(1 + y\frac{12E}{b^2 + d^2}\right), \tag{23}$$

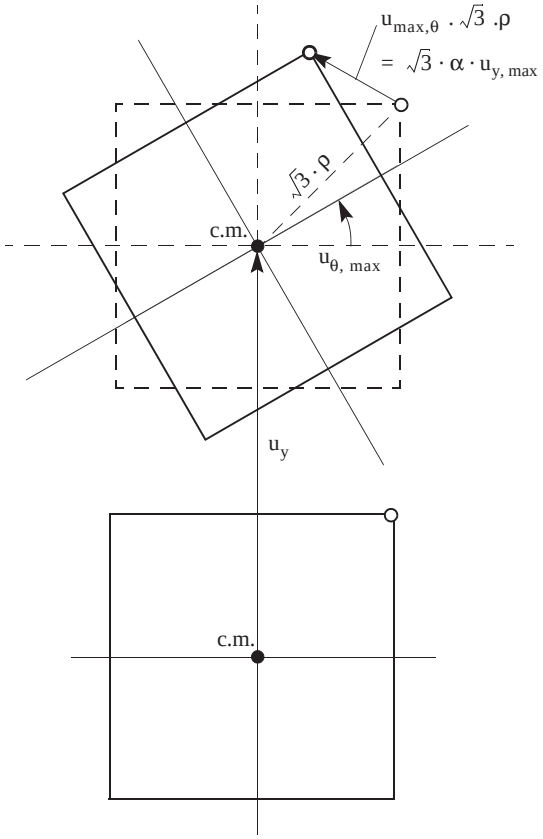

Fig. 16. Geometrical interpretation of the α parameter.

where D_M is the maximum displacement at the center of rigidity of the isolation system in the direction under consideration, E the actual (absolute) system eccentricity (including 5% accidental eccentricity), y the distance between the center of rigidity of the isolation system and the element of interest, measured perpendicular to the direction of seismic loading under consideration; and b, d are the shortest and longest plan dimensions of the structure, respectively.

Assuming a rectangular plan of dimensions $b \times d$ and a uniform distribution of the isolators, it can be shown that

$$|u_\theta|_{\max-\mathrm{IBC}} = \frac{12D_M E}{b^2+d^2} \cong \frac{12E}{b^2+d^2}|u_y|_{\max} = \sqrt{12}e\frac{|u_y|_{\max}}{\rho} = \alpha_{\mathrm{IBC}}\frac{|u_y|_{\max}}{\rho}, \tag{24}$$

where

$$\alpha_{\mathrm{IBC}} = \sqrt{12}e. \tag{25}$$

It is observed that unlike the proposed rotational "alpha" parameter, the one implied by the IBC provisions depend only on the relative eccentricity "e" and not on structural parameter "γ".

Using Eqs. (14), (17c) and (17f), the ratios of the undamped (α_u) and damped (α_d) rotational "alpha" parameter of the proposed method to that implied by the IBC provisions are obtained as

$$\alpha_u/\alpha_{\mathrm{IBC}} = \frac{2e}{\sqrt{(\gamma^2-1)^2+48e^2}}, \tag{26}$$

$$\alpha_d/\alpha_{\mathrm{IBC}} = -0.25 + \frac{3.26}{\gamma^2} - \frac{10e}{\gamma^4} \quad (\text{for } \xi = 5\%), \tag{27}$$

$$\alpha_d/\alpha_{\mathrm{IBC}} = -0.1 + \frac{2.15}{\gamma^2} - \frac{6e}{\gamma^4} \quad (\text{for } \xi = 10\%). \tag{28}$$

The above three ratios are plotted in Fig. 17. It is observed that for large values of "γ" and especially for large values of "γ" combined with large values of the relative eccentricity "e", the

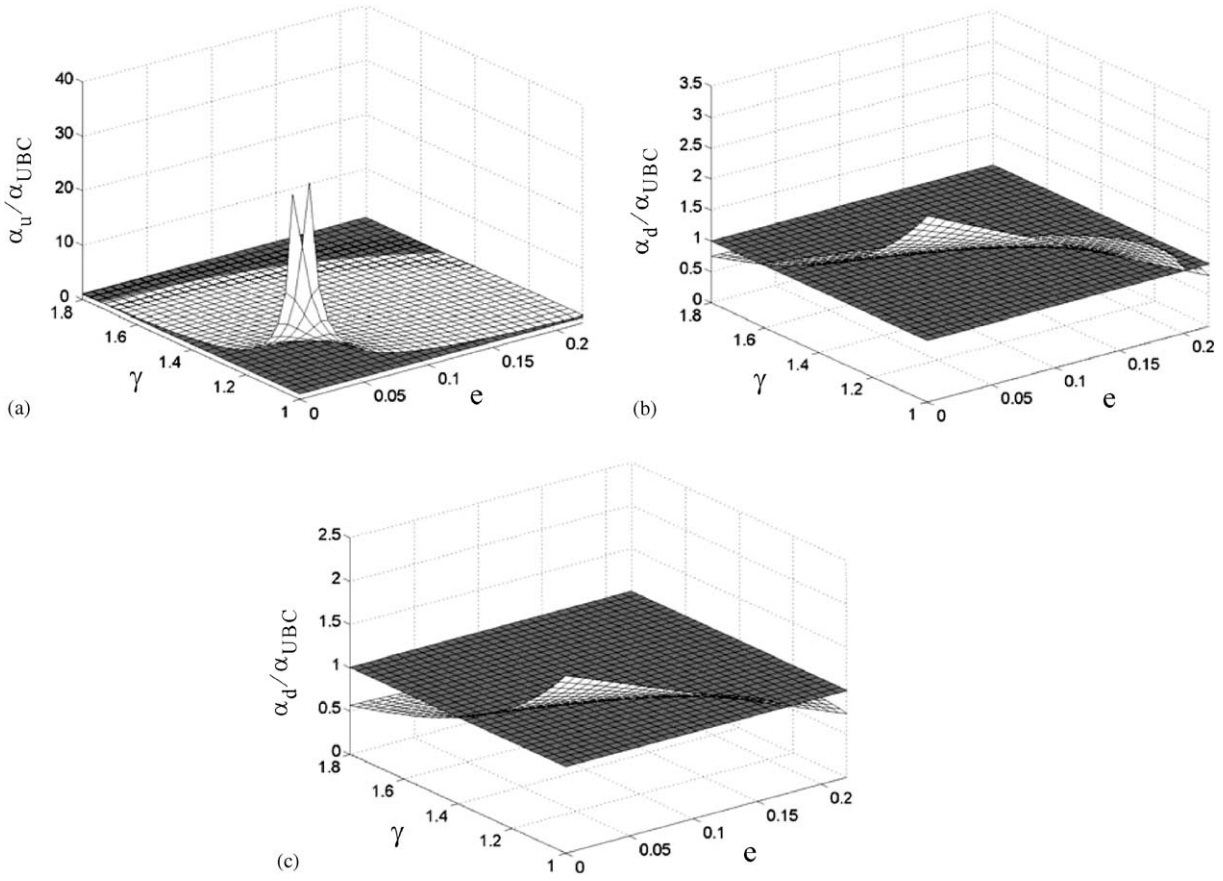

Fig. 17. Comparison of rotational "alpha" parameter of proposed method with that implied by the IBC provisions: (a) $\alpha_u/\alpha_{\mathrm{IBC}}$, (b) and (c) $\alpha_d/\alpha_{\mathrm{IBC}}$ for 5% and 10% damping ratio, respectively.

rotational "alpha" parameter of the proposed method is significantly smaller than its IBC counterpart. On the contrary, for small values of "γ" and especially for small values of "γ" combined with small values of "e", the "alpha" parameter of the proposed method is significantly larger than its IBC counterpart.

11. Numerical verification of the "alpha" method

Numerical verification of the "alpha" method is performed through direct numerical integration of the equations of motion, Eq. (1), of linear elastic one-story 3-dof eccentric systems to obtain the "exact" maximum rotational response, $|u_\theta|_{\max}$. Estimation of $|u_\theta|_{\max}$ through Eq. (22) requires numerical evaluation of the dimensionless rotational parameter α and of $|u_y|_{\max-\mathrm{ne}}$. In each case described below, parameter α is evaluated using either the closed-form expression in Eq. (14) for undamped systems or the empirical analytical expressions in Eq. (16) for damped systems. For each earthquake record considered in this study, the response parameter $|u_y|_{\max-\mathrm{ne}}$ is obtained through numerical integration of the equation of motion of an sdof oscillator of the same mass and uncoupled lateral stiffness as the eccentric system.

The same set of 125 earthquake records used in Section 8 is used in the numerical verification study. The eccentric systems considered here are characterized by the following wide ranges of structural parameter values: relative eccentricity "e" varying between 0% and 24% ($0 \leqslant e \leqslant 0.24$), modal damping ratio varying between 5% and 15% ($0.05 \leqslant \xi \leqslant 0.15$), $\gamma = \omega_\theta/\omega_L$ varying between 1.18 and 1.73 ($1.18 \leqslant \gamma \leqslant 1.73$). These ranges of parameter values cover the majority of cases of seismic isolated structures [6]. Fig. 18 is similar to Fig. 13 with $\rho|u_\theta|_{\max}/|u_y|_{\max}$ replaced by $\rho|u_\theta|_{\max}/|u_y|_{\max-\mathrm{ne}}$ and the addition of α_{IBC}. Figs. 19(a)–(f) compare the "exact" maximum rotational response (in radians) with the corresponding estimations obtained using (a) the "alpha" method (using both the alpha damped and alpha undamped parameters), (b) the SRSS method of modal combination [29], and (c) the method proposed by the International Building Code (IBC) (formerly Uniform Building Code (UBC)) [6,31]. Note that in the cases presented in Figs. 19(a)–(f), the "alpha" method provides an estimation of the maximum rotational response that is comparable or superior in accuracy to the estimation obtained via the SRSS method of mode combination. It is also observed that in general the estimation according to the IBC overestimates the maximum rotation developed by structures characterized by large values of "γ" and "e" as shown in Fig. 18 and illustrated in Figs. 19(e), (c), and (f). Conversely, it underestimates (up to several fold) the maximum rotation developed by structures characterized by low damping and small values of "γ" and "e" as shown in Fig. 18 and illustrated in Fig. 19(a). On the other hand, for large values of "γ" and "e" and for large damping ratio (e.g., $\xi = 15\%$), the IBC provisions may overestimate the maximum rotational response by a factor of two as illustrated in Figs. 19(e) and (f).

In summary, the above comparative numerical results together with other results not presented here show that (1) the "alpha" method is sufficiently accurate for engineering purposes and (2) the "alpha" method provides a maximum rotational response estimation of comparable accuracy with that given by the SRSS method. However, the "alpha" method has the following advantages over the latter: (1) it reduces the 3D problem to that of an sdof system and a simple calculation/

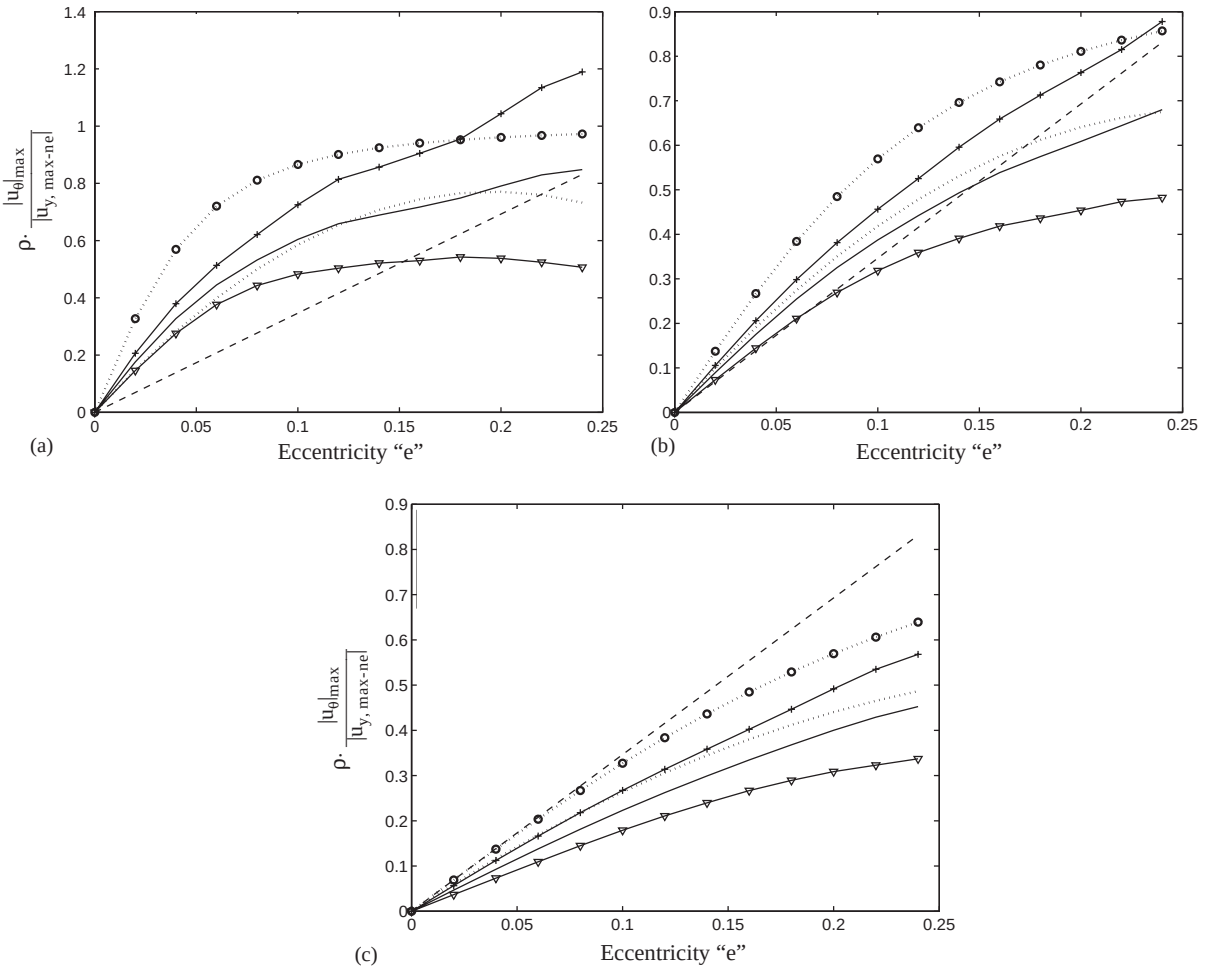

Fig. 18. Values of $\rho|u_\theta|_{\max}/|u_{y,\max-\mathrm{ne}}|$ as a function of the relative eccentricity "e" obtained from earthquake response simulations based on a set of 125 historical earthquake input records (all structures are characterized by $\xi = 4\%$): (a) $\gamma = 1.18$; (b) $\gamma = 1.41$; (c) $\gamma = 1.73$; —, mean; —+—, mean + one s.d.; —▽—, mean − one s.d.; -··◯··-, alpha (undamped); - - - - -, alpha (damping = 4%); – – –, alpha (according to IBC).

estimation of the structural "γ" parameter[10] and the relative eccentricity "e" to be used in a simple code-like formula to estimate the maximum rotational response, (2) for a given linear elastic 3-dof eccentric system, it provides, at minimum computational cost, immediate insight into the heart of the lateral torsional coupling problem and the resulting effects on the maximum deformation response of the system due to earthquake excitation (e.g., quick comparison of alternative design solutions[11] and direct estimation of additional deformation in corner isolators due to rotational

[10]For fairly regular structures, γ can be evaluated directly from the basic layout of the eccentric system through simple exact and/or approximate formulas.

[11]Since it is bounded between 0 (non-eccentric case) and 1, the rotational parameter α can be readily used as a formal index for the tendency of a given structure to develop a rotational response under dynamic excitation.

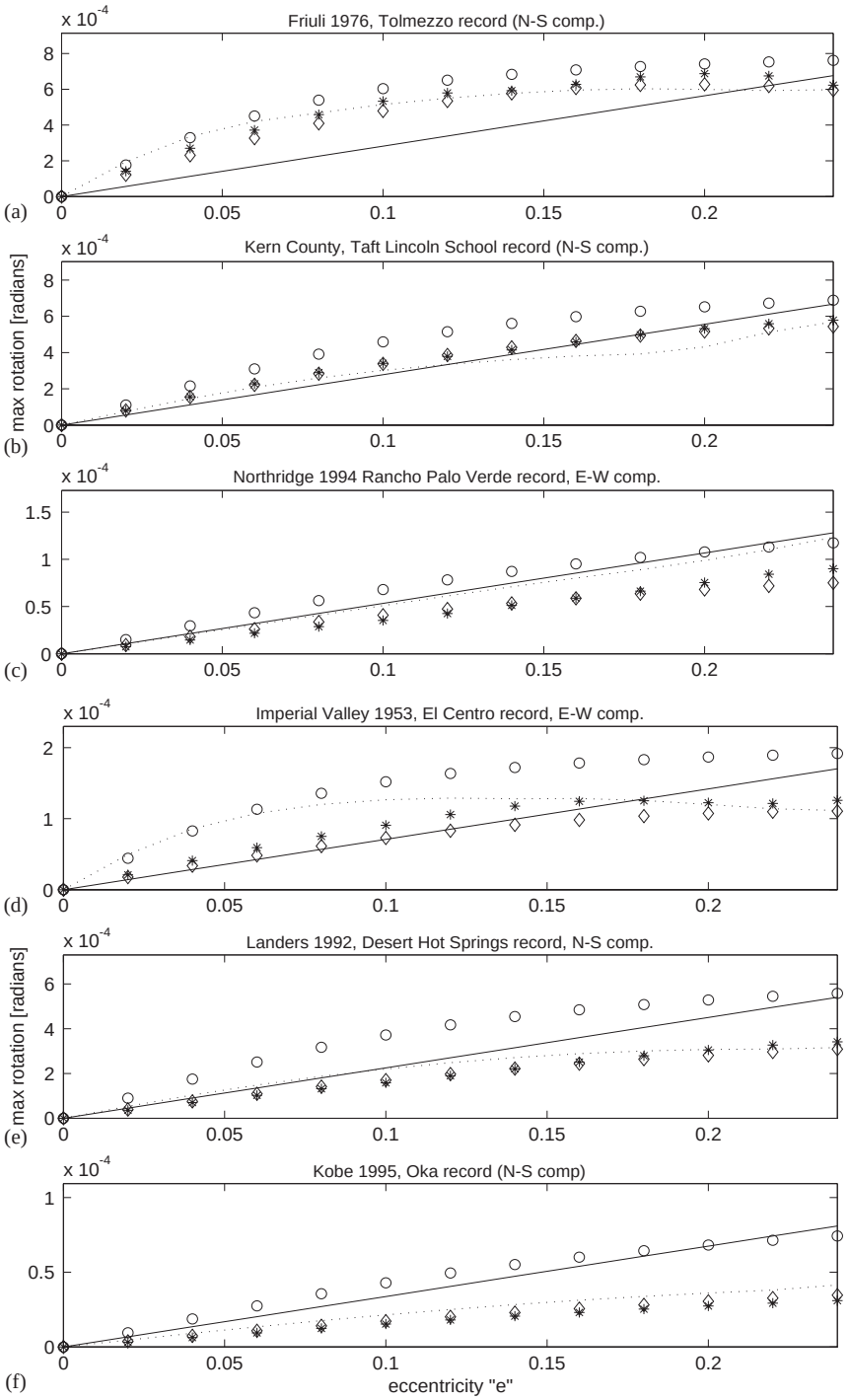
x 10^-4
Friuli 1976, Tolmezzo record (N-S comp.)
(a)
Kern County, Taft Lincoln School record (N-S comp.)
max rotation [radians]
(b)
Northridge 1994 Rancho Palo Verde record, E-W comp.
(c)
Imperial Valley 1953, El Centro record, E-W comp.
(d)
Landers 1992, Desert Hot Springs record, N-S comp.
(e)
Kobe 1995, Oka record (N-S comp)
(f)
eccentricity "e"

response effects), and (3) it is perfectly suited for the incorporation of accidental eccentricity in seismic design. The above numerical verification shows that in general, the rotational "α" parameter obtained from the proposed simplified method is more accurate than the current IBC provisions, which do not account for structural parameter "γ". The dependence of the maximum rotational response on parameter "γ" has already been recognized indirectly and qualitatively (on a case-by-case basis) by other researchers [2,3,12,22]. Thus, the present work formalizes into a simple, physically based formula the behavioral trends identified in previous research work and represented graphically in Fig. 12.

12. Experimental verification of the "alpha" method

Experimental verification of the "alpha" method consisted of a suite of shaking table tests performed on the medium size shaking table in the Department of Structural Engineering at Rice University in Houston, Texas. A versatile small-scale one-story 3-dof building model able to simulate a wide range of eccentric conditions was designed and constructed specifically for these tests.

12.1. Targeted prototype structure

In order to design and fabricate a meaningful small-scale model representative of a real seismic isolated building, a prototype structure was selected. A target prototype structure consisting of a four-story building 20 m × 20 m in plan and resting over 25 base isolators located at the nodes of a square 5 m × 5 m grid as shown in Fig. 20 is considered in this study, as it represents a reasonable example of seismic isolated building structure [6]. Considering a distributed mass of 1000 kg/m^2 for each floor, the inertia characteristics of the target prototype structure are:

- total mass of the superstructure: $m = 2 \times 10^6$ kg;
- polar mass moment of inertia of the superstructure with respect to the center of mass: $I_P = 1.\bar{3} \times 10^8$ kg m^2;
- mass radius of gyration of the superstructure with respect to the center of mass: $\rho = 8.16$ m. Assuming an uncoupled lateral natural period of vibration of $T_L = 2$ s for the target prototype structure, the following prototype characteristics can be deduced:
- lateral stiffness (in any direction) of the 25 isolators combined: $k = 2 \times 10^7$ N/m;
- rotational stiffness of the total base isolation system about the center of mass: $k_{\theta\theta} = 2 \times 10^9$ N m/rad;

Fig. 19. Maximum rotation response versus eccentricity "e" for several earthquake excitations and dynamic systems: (a) Friuli 1976 Tolmezzo record (N–S comp.), $\gamma = 1.18, \xi = 5\%$; (b) Kern County 1952 Taft Lincoln School record (N–S comp.), $\gamma = 1.41, \xi = 5\%$; (c) Northridge 1994 Rancho Palos Verdes record, (E–W comp.), $\gamma = 1.73, \xi = 5\%$; (d) Imperial Valley 1953 El Centro record (E–W comp.), $\gamma = 1.18, \xi = 15\%$; (e) Landers 1992 Desert Hot Springs record (N–S comp.), $\gamma = 1.41, \xi = 15\%$; (f) Kobe 1995 Oka record (N–S comp.), $\gamma = 1.73, \xi = 15\%$; SRSS estimation (- - - -), IBC estimation (—), "alpha damped" estimation ($\diamond\diamond\diamond$), "alpha undamped" estimation ($\circ\circ\circ$), "exact" results from complete 3D time domain integration ($***$).

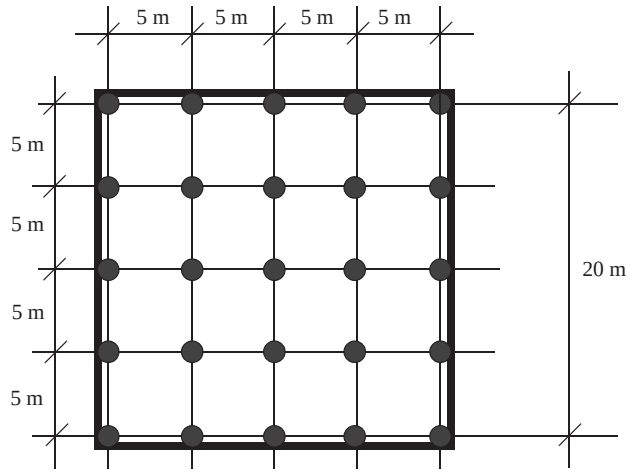

Fig. 20. Plan view of the prototype building.

- ratio of lateral to rotational natural period for zero eccentricity: $\gamma = \omega_\theta/\omega_L = \sqrt{k_{\theta\theta}/\rho^2 k} = 1.225$;
- rotational natural period of vibration for zero eccentricity: $T_0 = 1.632\,\text{s}$.

12.2. Model structure

12.2.1. Rationale

To accommodate the characteristics of the Rice University shaking table (on which these tests were performed) and for ease of model construction, model instrumentation, and response data acquisition, the time scale factor $\lambda_T = T_p/T_m = 5$ and the length scale factor $\lambda_L = L_p/L_m \cong 40$ were selected. Given the characteristics of the theory to be verified, we chose to construct a linear elastic one-story building model characterized by: (a) null longitudinal eccentricity ($e_y = 0$), (b) adjustable distance between the center of mass and the center of stiffness (i.e., system eccentricity) along the transversal (x-) direction, and (c) other dynamic characteristics which remain constant. Thus, the model had to satisfy the following requirements:

- maintain a linear elastic behavior throughout the shaking table tests;
- have a precisely located and fixed center of stiffness;
- have a precisely located and movable center of mass;
- have a precisely defined mass radius of gyration for the case of zero eccentricity;
- have a constant value of its uncoupled lateral natural period of vibration throughout the shaking table tests;
- have a constant value of the dimensionless structural parameter "γ".

In order to satisfy the above requirements, a model was built consisting of a carbon fiber sandwich plate supported by nine (three rows of three) solid plexiglas column rods fixed to both the carbon fiber top plate and a plexiglas base plate.

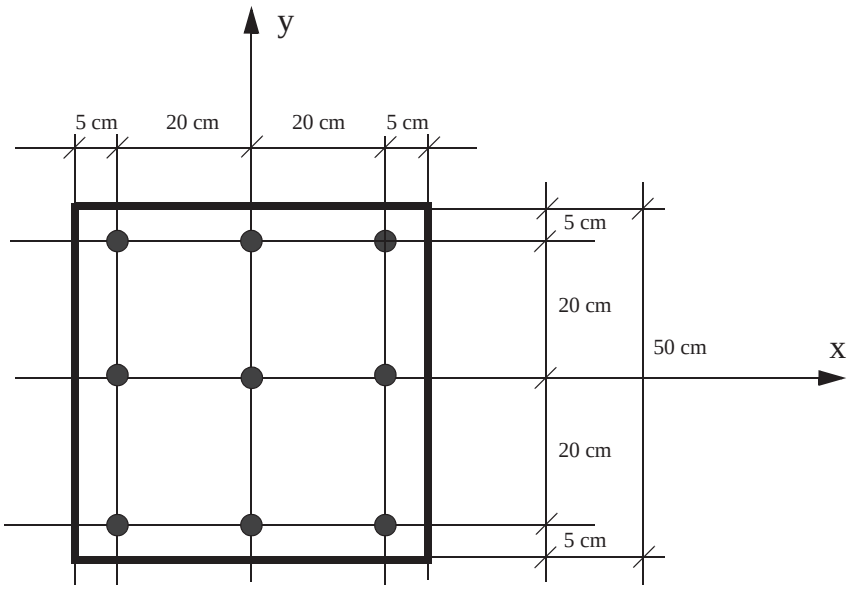

Fig. 21. Plan view of the model.

12.2.2. Design specifications

From the above scaling factors and requirements, the model must have an uncoupled lateral natural period of vibration of $T_L = 0.40$ s, a mass radius of gyration of about $\rho = 20.4$ cm, and a parameter $\gamma = 1.225$.

12.2.3. Weight and dimensions

The carbon fiber sandwich top plate is squared 50 cm × 50 cm in size, see Fig. 21, and weighs 0.550 kg. The nine plexiglas column rods are 6.35 mm in diameter, 225 mm in length and are located at the nodes of a 20 cm × 20 cm square grid. The plexiglas columns were sized, assuming a Young's modulus for the plexiglas of 294300 N/cm^2, to achieve a lateral stiffness of the model of 2000 N/m, which leads to a model uncoupled lateral natural period of 0.40 s for a total model mass of 8.00 kg. Particular attention (accuracy of location and consistency of clamping conditions) was paid to the connections of the column rods to both the top carbon fiber sandwich plate and the base plexiglas plate, so as to locate precisely the center of stiffness at the geometric center of the top plate.

Four weights of 1.850 kg each (including the clamping bolts) can be fixed to the top carbon fiber sandwich plate in various configurations as shown in Fig. 22. The locations at which these added weights could be positioned were carefully computed in order to obtain precisely transversal relative eccentricities of $e = e_x = 0\%, 2\%, \ldots, 18\%$, and 20% of the equivalent diagonal D_e as defined in Section 2, while maintaining a constant value of parameter $\gamma = 1.225$. Hooks and mounts for the displacement and acceleration transducers,[12] with a total weight of approximately

[12]The string potentiometers used as displacement transducers were located externally to the model.

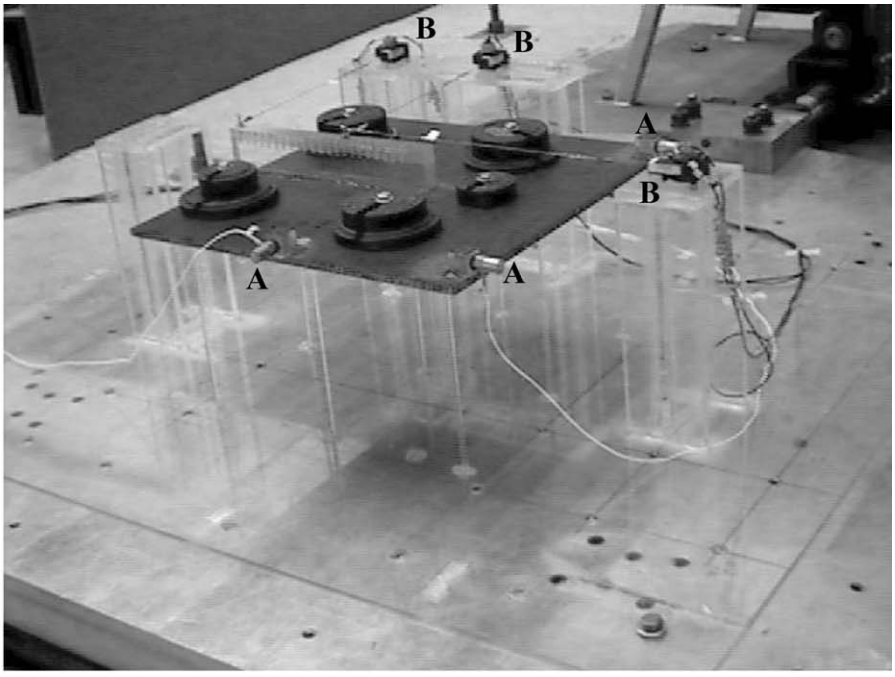

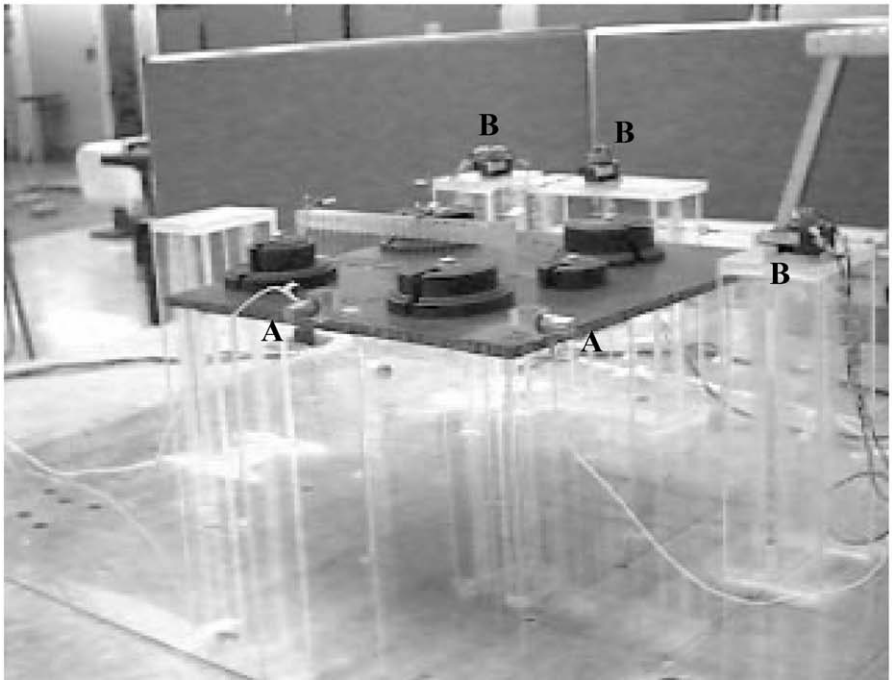

Fig. 22. The reduced scale model as built.

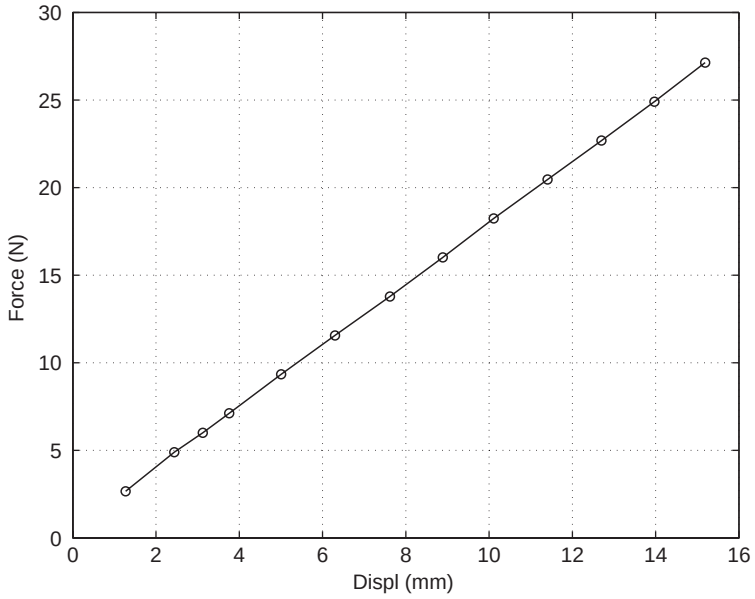

Fig. 23. Static load–deflection curve of the reduced scale model.

1.100 kg,[13] were attached to the top carbon fiber sandwich plate. Their positions and masses were taken into account in determining the precise clamping locations of the added weights. The resulting total mass of the model (neglecting the weight of the column rods) amounts to 9.05 kg, 13% in excess of the target 8.0 kg mass. Photographs of the model as built are shown in Fig. 22.

12.3. Static characteristics of the model

The model was first subjected, through a weight and pulley system, to a monotonically increasing horizontal static load up to 27.1 N applied at the center of stiffness in the longitudinal (y-) direction in order to determine the experimental static load–displacement curve shown in Fig. 23. This maximum static equivalent lateral force was selected based on a predicted absolute lateral acceleration response of the model of 0.3 g, which corresponds to a peak table acceleration of 0.10 g (= peak ground acceleration in the model world) and a dynamic amplification factor of 3. It is observed from Fig. 23 that the model behaves linearly up to at least 15.2 mm of lateral deformation. The experimental lateral stiffness amounts to 1800 N/m, which is close to the target value of 2000 N/m. This 10% reduction in the lateral stiffness is mainly due to the imperfect clamping of the plexiglas column rods.

[13]This weight also includes an additional mass used to cancel the mass eccentricity caused by the hooks and mounts for the displacement transducers and accelerometers.

12.4. Instrumentation and data acquisition for dynamic measurements

In order to measure the dynamic response of the physical model described above, a set of three string potentiometers and a set of three piezoelectric accelerometers were used as shown in Fig. 22. Each of these two sets of transducers is sufficient to completely determine the measured in-plane response (either displacement or acceleration) of the rigid top plate along the 3 dofs $u_x(t), u_y(t)$, and $u_\theta(t)$, at the (adjustable) center of mass of the eccentric system. Special rigid mounts in plexiglas were fixed on the base plate of the model to provide the necessary reference points to measure the relative displacement response of the top plate with respect to the base. The uniaxial shaking table displacement and acceleration were also measured through the built-in shaking table actuator LVDT and an additional accelerometer, respectively. All these transducers outputs were acquired at a sampling rate of 4 kHz through a LabView-controlled dynamic signal acquisition board hosted in a Pentium computer.

12.5. Dynamic characteristics of the model

In order to determine the actual dynamic characteristics of the model, a series of dynamic experiments were performed including both snap-back (free vibration) tests and white noise base excitation tests using the shaking table.

Fig. 24 shows the experimentally identified transfer function (both magnitude and phase) between base acceleration and roof (top plate) acceleration of the model in the longitudinal (y-) direction for null eccentricity condition. This transfer function was obtained through a white noise base excitation test and using the Bartlett's procedure of spectral estimation [33,34]. The resonant frequency is located at $f_L = \omega_L/(2\pi) = 2.2$ Hz, which corresponds to the actual uncoupled lateral natural frequency of vibration of the model. Using the half-power bandwidth method [29], the damping ratio of the system in the uncoupled longitudinal mode of vibration is estimated at about 6%.

Fig. 25 represents the Fourier amplitude spectrum of the free vibration rotational response of the model induced by an initial rotational deformation for null eccentricity condition. The spectral peak in the Fourier amplitude spectrum provides the actual uncoupled rotational natural frequency at $f_\theta = \omega_\theta/(2\pi) = 2.75$ Hz. The above experimentally identified uncoupled longitudinal and rotational natural frequencies of vibration allow the experimental determination of the structural parameter $\gamma = \omega_\theta/\omega_L = f_\theta/f_L = 2.75/2.2 = 1.25$, which is very close to the target design value of $\gamma = 1.225$.

12.6. Comparison between target and actual model characteristics

The actual uncoupled lateral natural frequency of the model is 2.2 Hz, which is 12% lower than the corresponding target design value due to the smaller stiffness and larger mass of the model as compared to the target design values. The time scaling factor $\lambda_T = 5$ selected for this experimental dynamic study gives a prototype uncoupled lateral natural frequency of 0.44 Hz. This prototype dynamic characteristic, although differing from the targeted prototype value of 0.5 Hz, is nonetheless still representative of common real seismic isolated buildings, which validates the model constructed for the purpose of the present investigation.

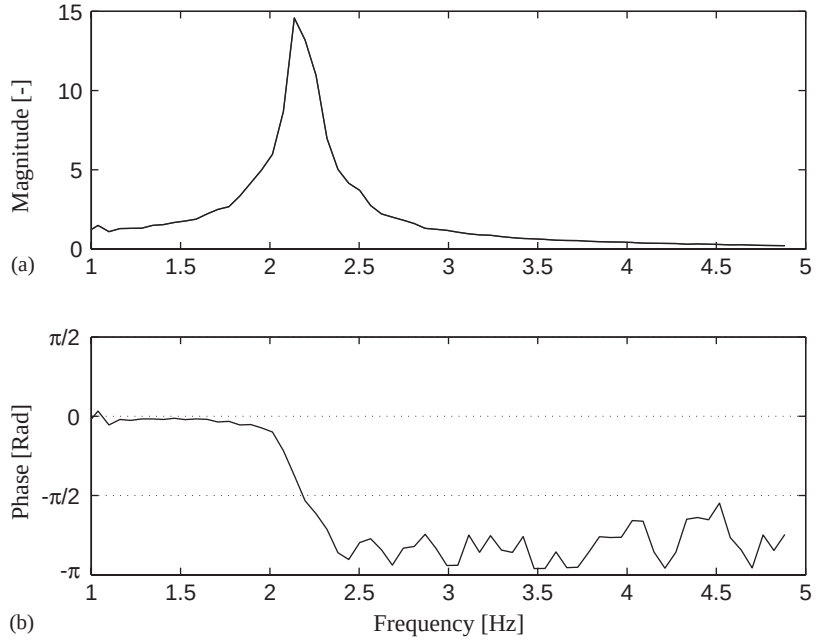

Fig. 24. Experimentally identified (a) magnitude and (b) phase transfer functions of the reduced scale model for decoupled longitudinal vibration (eccentricity = 0).

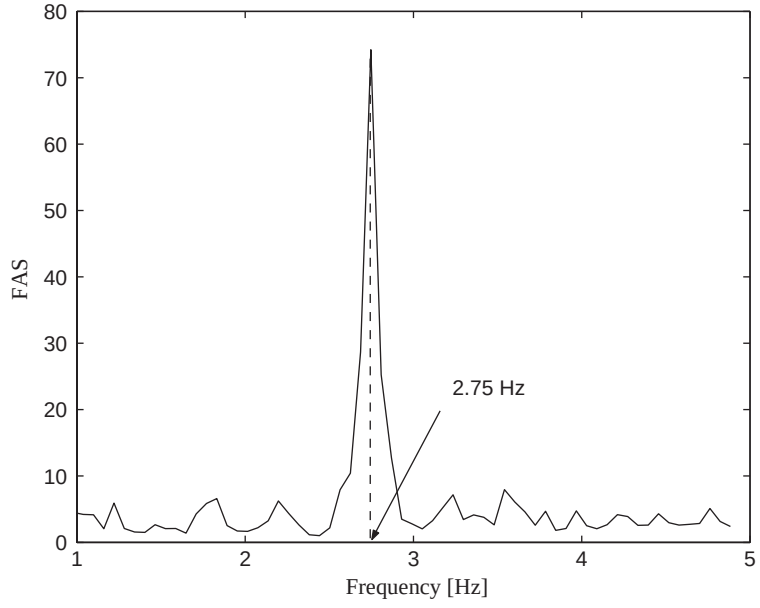

Fig. 25. Fourier amplitude spectrum (FAS) of free vibration (decoupled) rotational response of the reduced scale model for zero eccentricity condition.

The actual effective mass radius of gyration of the model is evaluated from the theoretical expression $\gamma = \sqrt{k_{\theta\theta}/(\rho^2 k)}$ using:

- the experimentally identified γ parameter ($\gamma = 1.25$);
- the experimentally identified value of the total lateral stiffness k; and
- the value of the torsional stiffness defined as $k_{\theta\theta} = \sum_{i=1}^{9} k_i r_i^2$ where k_i denotes the lateral stiffness of a single column (base isolator) and r_i is the distance between the ith column and the center of mass of the system. Here, the lateral column stiffness k_i is taken as one-ninth of the experimentally identified total lateral stiffness k.

The above evaluation procedure gives an actual effective mass radius of gyration of the model of $\rho^m = 19.0\,\text{cm}$ as compared to a target design value of 20.4 cm. Preserving the length scale factor $\lambda_L = 40$, it follows that the prototype mass radius of gyration is $\rho^p = 7.60\,\text{m}$ instead of the initial targeted value of 8.16 m.

12.7. Testing procedure

The small-scale model was tested on the Rice University uniaxial shaking table controlled to reproduce the following eight earthquake records: Imperial Valley 1940 (El Centro record, N–S comp.), Parkfield 1966 (Cholame # 2 record, E–W comp.), Friuli 1976 (Breginj record, N–S comp.), Friuli 1976 (Tolmezzo record, N–S comp.), Montenegro 1979 (Bar record, E–W comp.), Montenegro 1979 (Petrovac record, N–S comp.), Irpinia 1980 (Brienza record, N–S comp.), and a synthetic earthquake record compatible with the european seismic code (Eurocode8) design response spectrum. All these earthquake records were scaled both in time and amplitude. Note that different length scalings were used for the selected earthquake records, so as to obtain scaled table acceleration records with a peak acceleration in the range between 0.1 and 0.15 g. This range was selected in order to induce a relative displacement response of the model that is large enough to be measured accurately by the displacement transducers, but small enough not to threaten the structural integrity of the model. The model was tested for the aforementioned eight earthquake records and for the 11 added weight configurations corresponding to a transversal relative eccentricity from 0% to 20% with an increment of 2%. Thus, a suite of 88 shaking table tests was performed for the experimental verification of the "alpha" method. The eight earthquake records as reproduced by the Rice University shaking table are shown in Fig. 26.

12.8. Test results

As the main objective of the experimental tests is to validate the accuracy and robustness of the proposed simplified method, the maximum rotational response determined experimentally, $|u_\theta|_{\max-\exp}$, was compared with the corresponding estimation obtained using Eq. (22) where $|u_y|_{\max-\text{ne}}$ was also determined experimentally by testing the structural model under condition of null eccentricity. Notice that in Eq. (22), $|u_y|_{\max-\text{ne}}$ together with the mass radius of gyration ρ can be introduced either at the prototype or at the model level; the rotational response $|u_\theta|_{\max}$ in radians is the same at the prototype and model levels. Given the experimentally identified damping ratio $\xi = 6.0\%$, Eq. (17d) is used to estimate the "α" parameter in Eq. (22) for all tests performed.

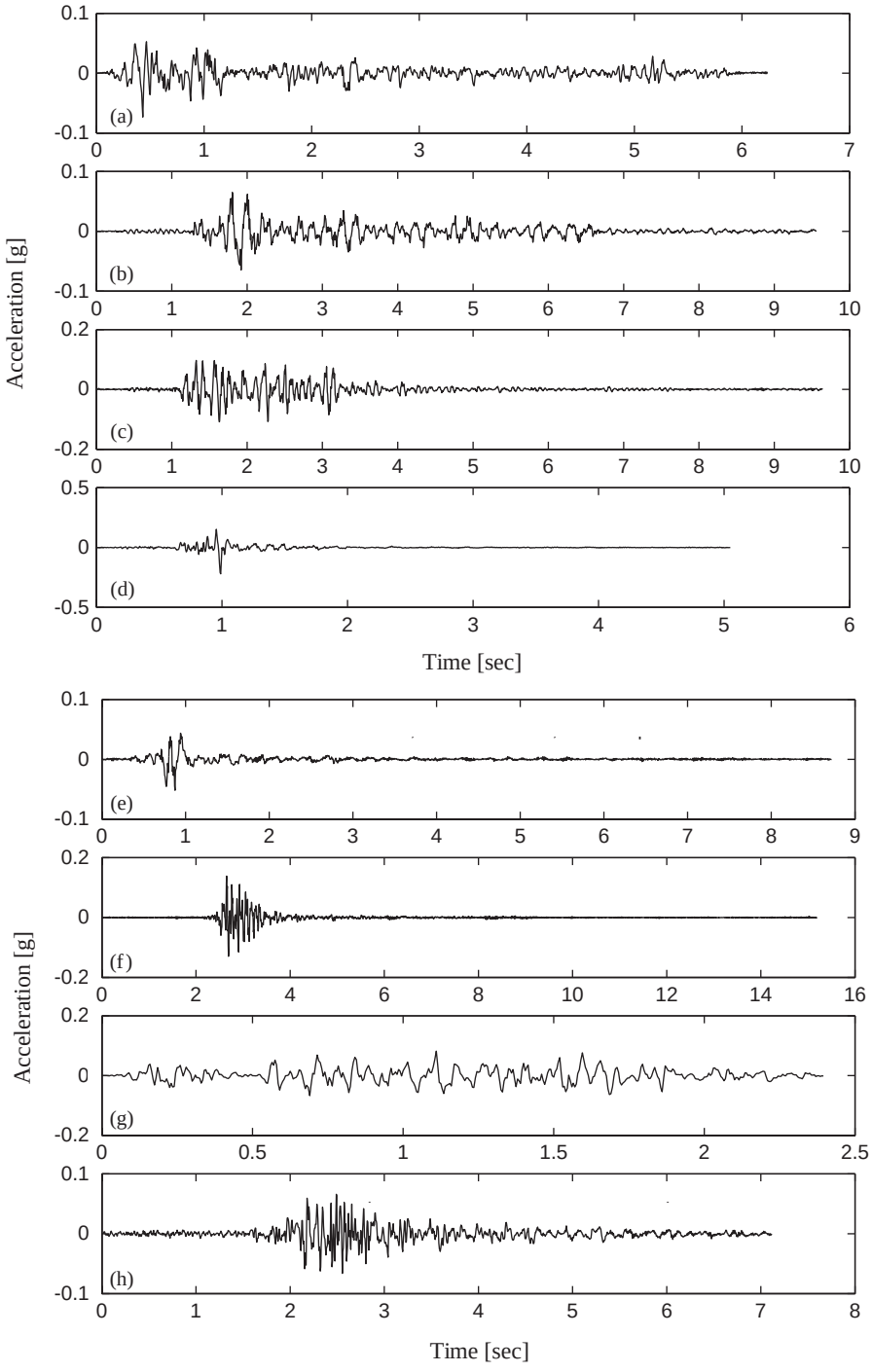

Fig. 26. Earthquake records (as reproduced by the shaking table): (a) Imperial Valley 1940, El Centro Record N–S comp.; (b) Montenegro 1979, Bar record E–W comp.; (c) Montenegro 1979, Petrovac record N–S comp.; (d) Friuli 1976, Breginj record N–S comp.; (e) Parkfield 1966, Cholame record, E–W comp.; (f) Friuli 1976, Tolmezzo record, N–S comp.; (g) Synthetic earthquake (EC8 spectrum compatible); (h) Irpinia 1980, Brienza record, N–S comp.

12.8.1. Measured maximum rotations and corresponding estimations provided by the proposed simplified ''alpha'' method

Figs. 27(a)–(h) compare measured maximum rotational responses with their corresponding estimations obtained using the proposed ''alpha'' method and the IBC provisions as a function of the relative eccentricity ''e''. As in the numerical verification, it is found that the ''alpha'' method (with the alpha-damped parameter α_d) is sufficiently accurate for engineering purposes and is generally more accurate than the IBC provisions, except in the case of the Friuli Breginj record (Fig. 27(e)) which is a very short, impulsive strong ground motion (Fig. 26). For the structural parameter $\gamma = 1.25$ of the model, the ''alpha'' method (using α_d) is particularly accurate at levels of relative eccentricity ''e'' ranging from 0% to 8%. In most cases, the IBC provisions underestimate significantly the actual maximum rotational response. It is also observed that the ''alpha'' undamped method provides a conservative upper bound (envelope) for the maximum rotational response. Note in Figs. 27(a)–(h) the small but non-zero maximum rotational response obtained experimentally for zero nominal eccentricity due to a small accidental eccentricity of the model.

12.8.2. Other experimental results

In this section, a number of simplifying assumptions and behavioral trends used and identified in developing the simplified ''alpha'' method are verified experimentally.

Fig. 28 shows the measured maximum longitudinal displacement response, $|u_y|_{\max}$, at the center of mass of the model as a function of the transversal relative eccentricity ''e'' for each of the 8 earthquake records considered. It is observed that, for a given base excitation, $|u_y|_{\max}$ does not change significantly with increasing eccentricity ''e'' and can be reasonably approximated by the maximum longitudinal displacement response for null eccentricity, $|u_y|_{\max-\mathrm{ne}}$. Note the similarities between the experimental results in Fig. 28 and the corresponding numerical simulation results shown in Fig. 15.

Fig. 29 compares the values of the rotational parameter ''α'' as obtained from Eq. (17d) with the corresponding values of $\rho \cdot |u_\theta|_{\max}/|u_y|_{\max-\mathrm{ne}}$ obtained experimentally and those obtained according to the IBC provisions. In all cases, except for the Friuli Breginj record, the proposed alpha-damped (α_d) parameter is in good agreement with the experimental results being close to their mean, while the alpha parameter recommended by the IBC provisions[14] generally underestimates the experimental results, especially for relative eccentricities ''e'' ranging from 0% to 10%. The alpha-undamped (α_u) parameter provides a conservative upper-bound (envelope) of the experimental results.

Figs. 30(a) and (b) show the free vibration rotational response (snap-back test) of the model with relative eccentricities of 2% and 4% of the equivalent diagonal D_e, respectively. Note the pronounced beating behavior in the free vibrational response, consistent with the analytical prediction given by Eq. (10c).

Figs. 31(a) and (b) display the free vibration longitudinal displacement response of the model structure with relative (transversal e_x) eccentricities of 2% and 4% of D_e, respectively, and null longitudinal eccentricity ($e_y = 0$). Note the absence of any visible beating phenomenon in these experimental longitudinal displacement responses, which is consistent with the analytical

[14] $\alpha_{\mathrm{UBC}} = \dfrac{|u_\theta|_{\max-\mathrm{by-UBC}} \cdot \rho}{|u_y|_{\max-\mathrm{ne-exp}}} = \sqrt{12}e.$

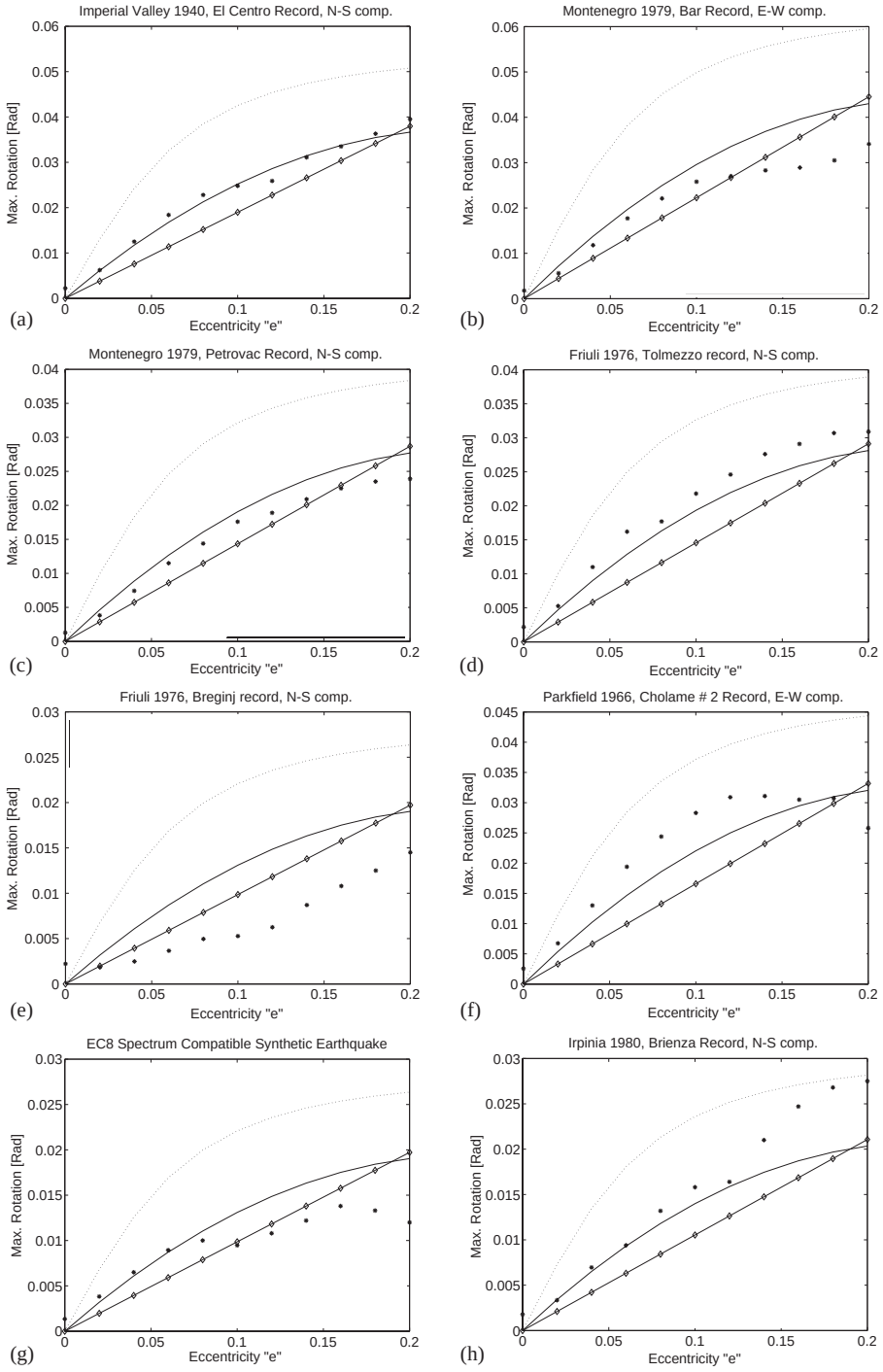

Fig. 27. Experimentally observed rotational responses (∗∗∗) and their corresponding estimations using the "α" method (—, alpha damped; - - - - -, alpha undamped) and using the IBC provisions (—◇—): (a) Imperial Valley 1940, El Centro Record N–S comp.; (b) Montenegro 1979, Bar record E–W comp.; (c) Montenegro 1979, Petrovac record N–S comp.; (d) Friuli 1976, Breginj record N–S comp.; (e) Parkfield 1966, Cholame record, E–W comp.; (f) Friuli 1976, Tolmezzo record, N–S comp.; (g) Synthetic earthquake (EC8 spectrum compatible); (h) Irpinia 1980, Brienza record, N–S comp.

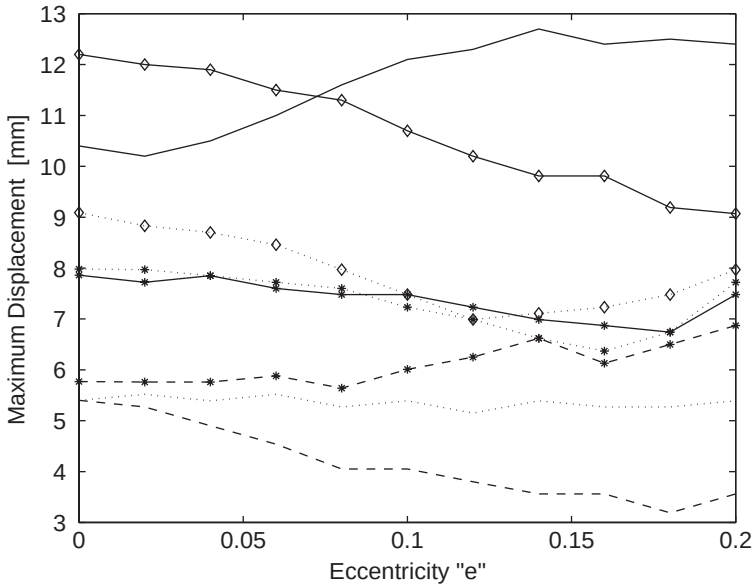

Fig. 28. Measured maximum longitudinal displacement at the center of mass of the reduced-scale model for increasing transversal eccentricity "e": —, Imperial Valley 1940; —◇—, Montenegro 1979—Bar record; —∗—, Montenegro 1979— Petrovac record; - - - - -, Friuli 1976—Breginj record; - -◇- -, Parkfield 1966; · · ·∗· · ·, Friuli 1976—Tolmezzo record; – – –, Synthetic earthquake record; – –∗– –, Irpina 1980—Brienza record.

prediction given by Eq. (10a) and the small value of the ratio A_3/A_1 for the present model as shown in Fig. 4 (where $F = e/(\gamma^2 - 1) = 1.778e$).

Fig. 32 plots the free vibration response (snap-back test) of the model in the u_y–u_θ plane for a relative transversal eccentricity "e" of 4% of D_e. It is observed that in every longitudinal response cycle, the maximum rotational response occurs almost concurrently with the maximum longitudinal response as discussed earlier in this paper. The strong similarities between the experimental results given in Fig. 32 and the numerical simulation results shown in Fig. 9 provides further validation of the theory presented earlier in the paper.

Fig. 33 compares free vibration (snap-back test) longitudinal and transversal responses of the model for a transversal relative eccentricity of 4% of D_e. Notice the presence of a very small transversal displacement response of the model, which can be due to a number of reasons such as (1) an imperfect initial deformation applied in the snap-back test (small x-component), (2) the presence of a small accidental eccentricity in the longitudinal (y-) direction of the model, and/or (3) the effects of the (small) restoring forces from the displacement transducers (string potentiometers). The theory presented earlier in the paper (Eq. (12b)) predicts zero transversal displacement response for null longitudinal eccentricity ($e_y = 0$) and an initial deformation along the longitudinal (y-) direction only, which is practically reproduced by the small-scale model.

Consistency between analytical predictions and experimental results shown in Figs. 30–33 further validate the construction of the small-scale model used for this experimental verification study.

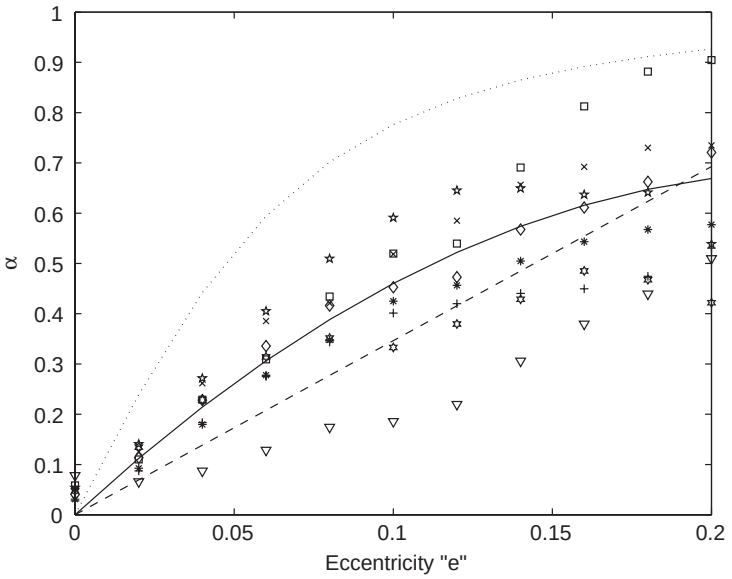

Fig. 29. Measured values of $\alpha = |u_\theta|_{\max}/|u_y|_{\max-\mathrm{ne}} \cdot \rho$ and corresponding predictions using the proposed simplified "alpha" method and the IBC provisions for increasing value of transversal eccentricity: - - - - -, alpha-undamped; —, alpha-damped; – – –, IBC provisions; ◇◇◇, Imperial Valley 1940; +++, Montenegro 1979—Bar record; ✻✻✻, Montenegro 1979—Petrovac record; ×××, Friuli 1976—Tolmezzo record; ▽▽▽, Friuli 1976—Breginj record; ☆☆☆, Parkfield 1966; ✡✡✡, synthetic earthquake record; □□□, Irpina 1980—Brienza record.

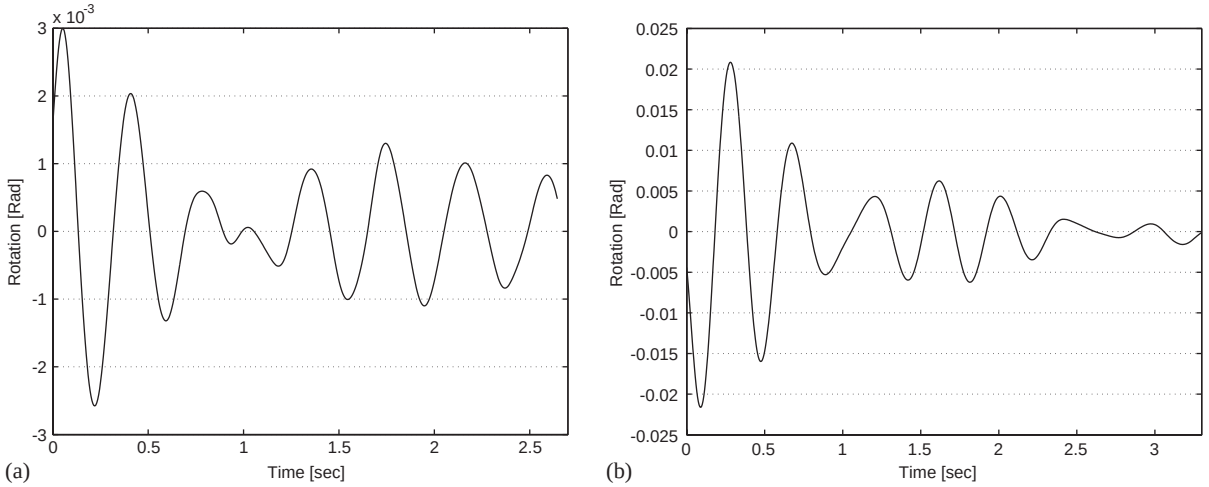

Fig. 30. Free vibration rotational response of model structure: (a) system eccentricity = 2% of D_e; (b) system eccentricity = 4% of D_e.

13. Conclusions

The analytical, numerical, and experimental investigations presented in this paper provide (a) new insight into the understanding of dynamic lateral–torsional coupling in linear elastic

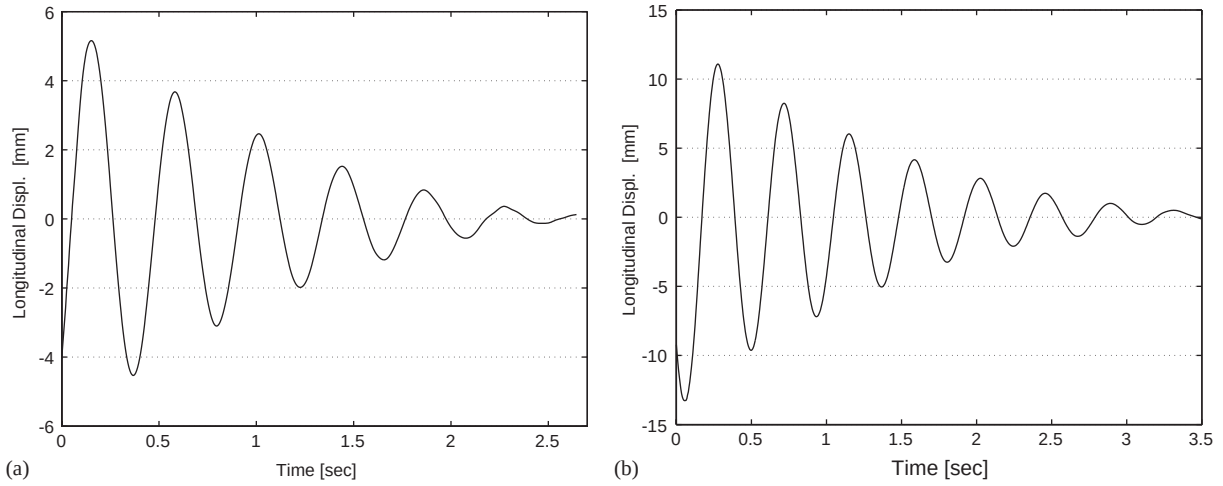

Fig. 31. Free vibration longitudinal displacement response of model structure: (a) system eccentricity = 2% of D_e; (b) system eccentricity = 4% of D_e.

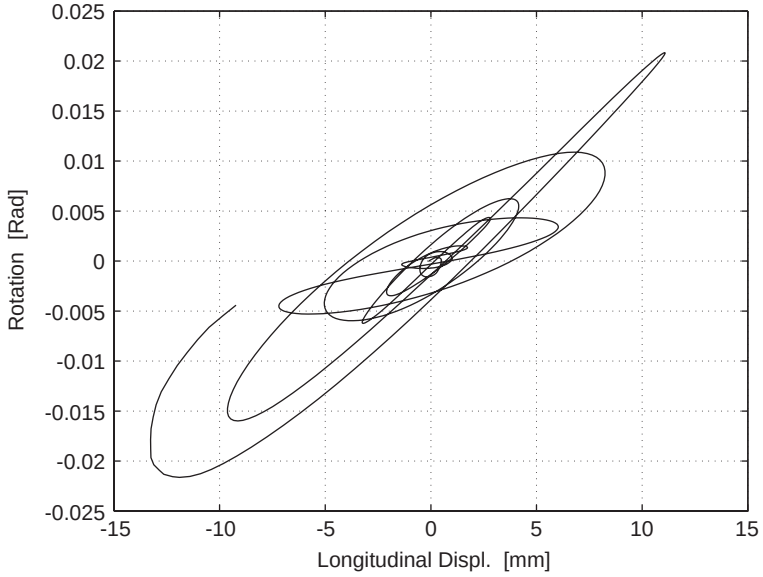

Fig. 32. Time evolution of rotation versus longitudinal displacement responses for the model structure in free vibration (system eccentricity = 4% of D_e).

one-story 3-dof eccentric systems, (b) sensitivity of coupled lateral–torsional response of eccentric structures to basic controlling system parameters, and (c) a new, physically based, simplified procedure to predict the maximum rotational response of eccentric systems.

In this paper, an important dimensionless response parameter, called the ''alpha'' parameter, is identified as the product of the mass radius of gyration of the structure and the ratio of the

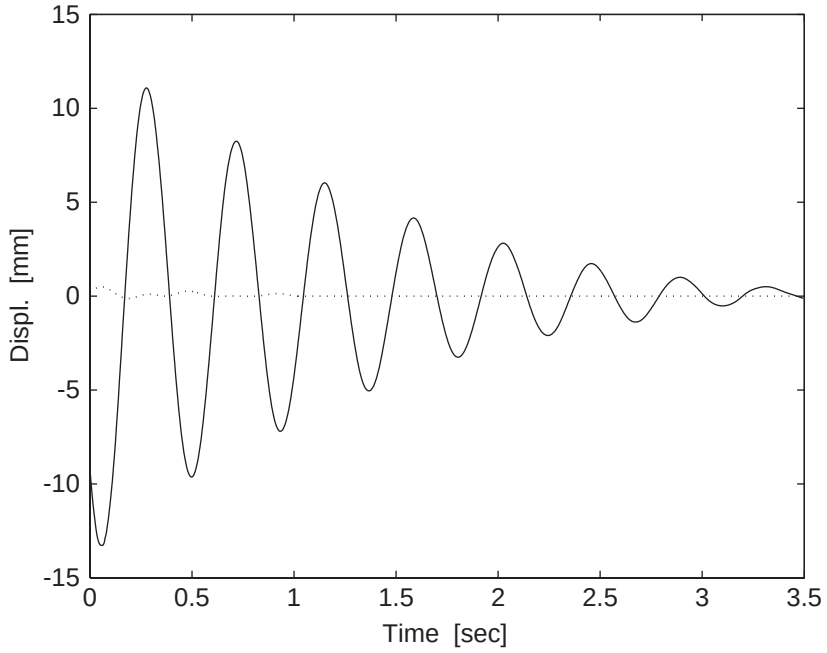

Fig. 33. Longitudinal displacement response (solid line) and transversal displacement response (dotted line), as developed by the model structure in free vibrations (system eccentricity = 4% of D_e).

maximum rotational to the maximum longitudinal displacement response developed by a one-story eccentric system in free vibration, i.e., $\alpha = \rho|u_{\theta,\max}/u_{y,\max}|_{fv}$. It is shown that the corresponding dimensionless parameter under forced vibration, $\rho|u_{\theta,\max}/u_{y,\max}|_{\text{forced}}$, is only weakly excitation dependent and therefore strongly system dependent.

The "alpha" parameter is shown to depend on only two system parameters, namely the relative eccentricity "e" of the system and $\gamma = \omega_\theta/\omega_L$ where ω_L is the lateral uncoupled natural circular frequency of the system and ω_θ is the natural circular frequency of rotational vibration of a corresponding non-eccentric structure. It is also shown that for undamped structures, the "alpha" parameter depends on "e" and "γ" through the single system parameter $F = e/(\gamma^2 - 1)$.

Structures characterized by large values of "alpha" are prone to develop large rotational dynamic response, while structures with small values of "alpha" are less prone to rotate when responding dynamically. Thus, sensitivity analysis of the "alpha" parameter with respect to physical structural parameters is crucial in understanding the dynamic behavior of laterally–torsionally coupled systems. Such sensitivity analysis was performed in the paper and the results are in agreement with past research work. For a specific structure, parameter "alpha" provides, at minimum computational cost, immediate insight into the heart of the torsional coupling problem.

A fundamental result was obtained, namely that parameter "alpha" has an upper bound of unity, thus limiting the maximum rotational response developed in free vibration from an imposed initial deformation by any eccentric, linear elastic one-story system to the maximum

longitudinal displacement at the center of mass divided by the mass radius of gyration of the structure (i.e. $|u_{\theta,\max}| \leqslant \frac{1}{\rho}|u_{y,\max}|$). Furthermore, since the rotational parameter "α" is bounded between zero (non-eccentric case) and unity, this parameter can be readily used as a formal index for the inherent property of a given structure to develop a rotational response under dynamic excitation.

The aforementioned unique properties of the "alpha" parameter form the basis of the proposed simplified analysis procedure, called the "alpha" method, presented in this paper. Using this procedure, the maximum rotational response of a given system due to seismic excitation can be estimated, through a simple code-like formula, as $|u_\theta|_{\max} = \alpha|u_y|_{\max-\mathrm{ne}}(1/\rho)$ where $|u_y|_{\max-\mathrm{ne}}$ is the maximum longitudinal displacement developed by an sdof oscillator of same mass and uncoupled lateral stiffness as the eccentric system. In the case of earthquake excitation, $|u_y|_{\max-\mathrm{ne}}$ can be readily obtained from a response spectrum [29]. A compact exact closed-form expression for the "alpha" parameter is given for the undamped case, and empirical analytical expressions based on least-squares fitting of numerical dynamic simulation data are provided for the damped case.

An extensive numerical verification of the "alpha" method was carried out based on a set of 125 historical earthquake records over a wide range of structural parameters encompassing the majority of design situations for seismic isolated structures.

An experimental verification was performed through snap-back and shaking table tests of a small-scale building model. A suite of 88 individual shaking table tests were performed using 8 historical and synthetic earthquake records appropriately scaled in time and amplitude. The test model, 50 cm × 50 cm in plan, was carefully designed for adjustable (between 0% and 20% of the equivalent diagonal D_e) transversal eccentricity between the center of mass and the center of rigidity and other dynamic characteristics kept constant. This model is representative of a realistic prototype seismic isolated structure consisting of a four story building, 20 m × 20 m in plan, with an uncoupled lateral natural period of 2.27 s.

The numerical and experimental verification results show that the "alpha" method (1) is sufficiently accurate for design purposes to estimate the maximum rotational response developed by an eccentric system under seismic excitation, (2) is on the average significantly more accurate than the current IBC provisions for base-isolated structures, which do not account for structural parameter γ and in the majority of cases considerably underestimates the maximum rotational response, (3) is robust to a wide range of variation of system parameters, and (4) is at least as accurate as the widely used SRSS modal combination method for maximum rotational response prediction. Furthermore, through its simple formulation, the "alpha" method can be readily and effectively used for practical design purposes and it is perfectly suited for the incorporation of accidental eccentricity (generally prescribed to $e = 3.5\%$ corresponding to 5% of the side of a structure square in plan) in seismic analysis and design.

The "alpha" method, even though specifically developed for seismic isolated structures, could also be applied to other structural systems such as one-story building structures with rotationally symmetric lateral stiffness and deepwater fixed offshore towers subjected to dynamic excitations such as earthquakes, earth tremors, wind-, fluid-, underground traffic-, and machine-induced vibrations.

Undergoing research by the first author indicates that the "α" parameter introduced in this paper for linear elastic eccentric one-story systems is larger than the corresponding "α" parameter

($= \rho|u_{\theta,\max}|/|u_{y,\max}|$) for nonlinear eccentric one-story systems made up of bilinear inelastic resisting elements (e.g., seismic isolators) [28].

Acknowledgements

Dr. Fausta Bacci, Dr. Stefano Silvestri, Dr. Lorenzo Altobelli and Prof. Claudio Ceccoli are gratefully acknowledged for the support and data analysis provided in the early stage of development of this new approach to the understanding and treatment of dynamic lateral–torsional coupling in eccentric structures. The support from Rice University for the construction of the small-scale model tested on the Rice University shaking table and the acquisition of the instrumentation to carry out the experimental verification study presented herein is gratefully acknowledged. The authors also wish to thank Prof. A.J. Durrani, Chairman of the Civil Engineering Department at Rice University, Houston, Texas, for his support and insightful suggestions provided in the course of this study.

References

[1] A. Rutenberg, State-of-the-art report—seismic nonlinear response of code-designed asymmetric structures, *The 11th European Conference on Earthquake Engineering, Behaviour of Irregular and Complex Structures*, EAEE Task Group (TG) 8, A.A. Balkema, Rotterdam, 1998.
[2] C.L. Kan, A.K. Chopra, Effects of torsional coupling on earthquake forces in buildings, *Journal of the Structural Division ASCE* 103 (4) (1977) 805–819.
[3] C.L. Kan, A.K. Chopra, Elastic earthquake analysis of a class of torsionally coupled buildings, *Journal of the Structural Division ASCE* 103 (4) (1977) 821–839.
[4] R. Hejal, A.K. Chopra, Earthquake response of torsionally coupled buildings, Report UCB/EERC-87/20, Earthquake Engineering Research Center, University of California, Berkeley, CA, 1987.
[5] S. Lu, W.J. Hall, Torsion in two buildings—1987 Whittier Narrows earthquake, *Earthquake Engineering and Structural Dynamics* 21 (2) (1992) 387–407.
[6] F. Naeim, J.M. Kelly, *Design of Seismic Isolated Structures—From Theory to Practice*, Wiley, New York, 1999.
[7] W.K. Tso, Static eccentricity concept for torsional moment estimations, *Journal of Structural Engineering ASCE* 116 (5) (1990) 1199–1212.
[8] R.K. Goel, A.K. Chopra, Inelastic seismic response of one-story, asymmetric-plan systems, Report UCB/EERC-90/14, Earthquake Engineering Research Center, University of California, Berkeley, CA, 1990.
[9] R.K. Goel, A.K. Chopra, Inelastic response of one storey, asymmetric-plan systems: effects of stiffness and strength distribution, *Earthquake Engineering and Structural Dynamics* 19 (3) (1990) 949–970.
[10] W.K. Tso, H. Ying, Additional seismic inelastic deformation caused by structural asymmetry, *Earthquake Engineering and Structural Dynamics* 19 (2) (1990) 243–258.
[11] S. Nagarajaiah, A.M. Reinhorn, M.C. Constantinou, Nonlinear dynamic analysis of 3D-base isolated structures, *Journal of the Structural Division ASCE* 117 (7) (1991) 2035–2054.
[12] M. De Stefano, G. Faella, R. Ramasco, Inelastic response and design criteria of plane-wise asymmetric systems, *Earthquake Engineering and Structural Dynamics* 22 (3) (1993) 245–259.
[13] J.C. Correnza, G.L. Hutchinson, A.M. Chandler, Effect of transverse load-resisting elements on inelastic earthquake response of eccentric-plan buildings, *Earthquake Engineering and Structural Dynamics* 23 (1) (1994) 75–89.
[14] J.L. Humar, P. Kumar, Effect of orthogonal in-plane structural elements on inelastic torsional response, *Earthquake Engineering and Structural Dynamics* 28 (10) (1999) 1071–1097.

[15] A.M. Chandler, G.L. Hutchinson, Code design provisions for torsionally coupled buildings on elastic foundation, *Earthquake Engineering and Structural Dynamics* 15 (1987) 517–536.
[16] A.M. Chandler, G.L. Hutchinson, Evaluation of code torsional provisions by a time history approach, *Earthquake Engineering and Structural Dynamics* 15 (1987) 491–516.
[17] A.M. Chandler, J.C. Correnza, G.L. Hutchinson, Seismic torsional provisions: influence on element energy dissipation, *Journal of Structural Engineering ASCE* 122 (5) (1996) 494–500.
[18] R.K. Goel, A.K. Chopra, Seismic code analysis of buildings without locating centers of rigidity, *Journal of Structural Engineering ASCE* 119 (10) (1993) 3039–3055.
[19] C.M. Wong, W.K. Tso, Evaluation of seismic torsional provisions in Uniform Building Code, *Journal of Structural Engineering ASCE* 121 (10) (1995) 1436–1442.
[20] W.K. Tso, R.S.H. Smith, Re-evaluation of seismic torsional provisions, *Earthquake Engineering and Structural Dynamics* 28 (1999) 899–917.
[21] M. De Stefano, A. Rutenberg, A comparison of the present SEAOC/UBC torsional provisions with the old ones, *Engineering Structures* 19 (8) (1997) 655–664.
[22] W.K. Tso, K.M. Dempsey, Seismic torsional provisions for dynamic eccentricity, *Earthquake Engineering and Structural Dynamics* 8 (1980) 275–289.
[23] S. Nagarajaiah, A.M. Reinhorn, M.C. Constantinou, Torsional coupling in sliding isolated structures, *Journal of the Structural Division ASCE* 119 (1) (1993) 130–149.
[24] S. Nagarajaiah, A.M. Reinhorn, M.C. Constantinou, Torsion in base isolated structures with elastomeric isolation systems, *Journal of Structural Engineering ASCE* 119 (10) (1993) 2932–2951.
[25] J.P. Stewart, J.P. Conte, I.D. Aiken, Observed behavior of seismically isolated buildings, *Journal of Structural Engineering ASCE* 125 (9) (1999) 955–964.
[26] F. Bacci, Comportamento Spaziale di Edifici Sismicamente Protetti con Isolatori, Tesi di Laurea, Universita' degli Studi di Bologna, Facolta' di Ingegneria, 1994.
[27] T. Trombetti, Un approccio semplificato all'analisi dei problemi torsionali negli edifici isolati sismicamente alla base, *Giornale del Genio Civile* 132 (1994) 10–12, 243–267.
[28] T. Trombetti, C. Ceccoli, S.A. Silvestri, A simplified approach to the analysis of torsional problems in seismic base isolated structures, *First International Conference of Structural Engineering and Construction ISEC-01*, A.A. Balkema, Rotterdam, 2001.
[29] A.K. Chopra, *Dynamics of Structures: Theory and Applications to Earthquake Engineering*, Second ed., Prentice-Hall, Englewood Cliffs, NJ, 1994.
[30] R.K. Goel, Simplified analysis of asymmetric structures with supplemental damping, *Earthquake Engineering and Structural Dynamics* 30 (9) (2001) 1399–1416.
[31] International Building Code, International Code Council, Inc., 2000.
[32] SEAOC, Recommended Lateral Force Requirements and Commentary, Seventh ed., 1999.
[33] D.H. Johnson, D.E. Dudgen, *Array Signal Processing—Concepts and Techniques*, Prentice-Hall, Englewood Cliffs, NJ, 1993.
[34] T.L. Trombetti, J.P. Conte, Shaking table dynamics: results from a test-analysis comparison study, *Journal of Earthquake Engineering* 6 (4) (2002) 513–551.